UNIVERSITY OF CALIFORNIA, SAN DIEGO

A BIOMEMETIC TRIPLE-ACTION HYBRID SYSTEM FOR ANTI-INFLAMMATION

A Thesis submitted in partial satisfaction of the requirements
for the degree, Master of Science

in

Chemical Engineering

by

Yu Fan

Committee in charge:

Professor Liangfang Zhang, Chair
Professor Yi Chen
Porfessor Jesse Jokerst

2017

The Thesis of Yu Fan is approved and it is acceptable in quality and form for publication on microfilm and electronically:

_____

_____

_____

Chair

University of California, San Diego

2017

Table of Contents

LIST OF FIGURES

ACKNOWLEDGEMENTS

I would like to acknowledge the chair of my thesis committee, Dr. Liangfang Zhang, for mentorship and the guidance given for the project.

I would like to acknowledge the lab supervisor, Dr. Weiwei Gao, for helping me plan the figures and solve critical problems encountered during the project.

I also want to acknowledge Yue Zhang, Qiangzhe Zhang, Xinxin Zhang, Pavimol Angsantikul, Hua Gong, Kevin Spiekermann for helping me with the experiments and generating some of the figures.

Finally, I would like to thank the entire Dr. Zhang's team for the overall help and support.

ABSTRACT OF THE THESIS

A BIOMEMETIC TRIPLE-ACTION HYBRID SYSTEM FOR ANTI-INFLAMMATION

by

Yu Fan

Master of Science in Chemical Engineering

University of California, San Diego, 2017

Professor Liangfang Zhang, Chair

Nanofibers have shown promising results as an excellent drug delivery platform and a wound healing medium due to their fibrous morphology and high porosity. They are also a highly versatile nanosystem with customizable material composition and surface structure. Recent emergence of the cell membrane cloaking technology and its

detoxification capability enabled a new way of nanofiber functionalization. The endotoxin and cytokine neutralizing properties of mouse J774 macrophage cell membrane coated nanoparticles (MϕNP) have previously been reported, but the nature of free nanoparticles prohibits local cytokine neutralization. Herein, we introduce a triple-action nanofiber-nanoparticle hybrid system that functions both as a drug delivery and a MϕNP retention platform. This project explored attaching MϕNP onto dual-drug loaded polycaprolactone (PCL) nanofiber surface. Our final nanoparticle-nanofiber hybrid system attenuates inflammation in three directions: curcumin reduces inflammation through modulating cytokine transcription; ciprofloxacin provides powerful anti-microbial effects; the attached MϕNPs show improved cytokine neutralization. The hybrid system serves as a new way to integrate traditional drug-delivery nano-platforms with the innovative biomimetic membrane toxin-neutralizing nanoparticles.

Introduction

Inflammation is an important process from the immune system when encountering external stimuli. During wound healing, inflammation helps recruit immune cells to the local wound site. The immune cells are responsible for secreting growth factors that promote cell proliferation and wound closure. However, in some cases, inflammation can also negatively impact wound healing. In the presence of endotoxin or bacteria, inflammation can go into a chronic state, which degrades growth factors. Hence, inflammation needs to be controlled in many cases. Efficient delivery of anti-inflammatory drugs has been studied extensively in research. The structure and the biocompatibility of the delivery medium is the key to effective drug delivery.

This Master thesis project explores the possibilities of using nanofibers as a drug delivery platform and a membrane NP retention scaffold to provide cytokine and endotoxin neutralization, anti-inflammatory and antibacterial activities, as well as possible wound healing efficacies. The project creates a nanofiber/nanoparticle hybrid system, which consists of multiple components that target different problems during wound healing. This system achieves the goals by attaching mouse J774 macrophage cell membrane coated PLGA nanoparticles (Macrophage NP) onto PCL nanofibers while simultaneously load curcumin and ciprofloxacin into the fibers. Macrophage NPs are responsible for cytokine and endotoxin neutralization as previously reported; curcumin provides anti-inflammatory properties; and ciprofloxacin, a common antibiotic, acts as a powerful anti-bacterial agent. Various specific experiments were designed to verify the role of each component.

Background

Nanofibers

The advancement in nanofabrication technologies allows production of polymer fibers in the submicron scale. Common fiber manufacturing techniques such as melt processing and electrospinning are able to produce polymer fibers ranging from a few microns to several nanometers in diameter. Extensive applications and intensive research on those thin materials have granted the fibers a unique name—nanofibers. Nanofibers are defined by any fibrous material with diameter in the nanoscale (typically less than 100 nm) (1). The term has later extended to also define submicron fibers that are more than 100 nm due to their similar physical properties with the thinner counterpart as well as their wide adoption in research and industry (1). Because of their high surface area to weight ratio, easy control of their functionality, high permeability and ease of production, nanofibers have been widely used in medical, energy, and many other fields in the industry (2).

Electrospinning is an extremely versatile and simplistic method to fabricate nanofibers using a broad spectrum of materials, including organic, inorganic, metals and metal oxides. Polymer is normally dissolved in organic solvents or melted into liquid state before loaded into the spinning equipment and used as the raw fiber material. A typical experimental setup consists of four main components: a syringe filled with dissolved or molten polymer solution, a syringe pump to ensure consistent delivery of the polymer solution, a conductive collector at a desired distance, and a high voltage power supply to apply an electric field between the metal tip and the collector 3 (Figure 1). The voltage for the electric field is generally high, (between 10-50 kV) (3). The principle of the

electrospinning technology is rather simple. Since the electrodes are applied between the blunted syringe needle and the collected, polymer solution coming out the tip becomes highly charged.

Although the components and operations of electrospinning are relatively simple, the mechanism of fiber formation is complicated and not fully understood. Two models have been developed through experimental observations are Taylor Cone and the jet flow instability (3). The two theories describe the spinning mechanism at the metal tip and during the flight towards collector, respectively. Other than the inherent surface tension on the face of the droplet, two major repulsive electrostatic forces will exert on the fluid droplet: surface charge electrostatic repulsion and Coulombic force from the electric field (4). Because of the electric field and the

resulting forces, the polymer droplet at the metal tip deforms into a conical shape, which has widely been referred to as the Taylor Cone (5). When the voltage increases, the repulsive forces will overpower the surface tension, a jet of polymer solution will burst out of the Taylor Cone and be pulled towards the fiber collector, which is served as the counter electrode (3). The jet will elongate and become thinner under electric field's strong driving force, and the organic solvent will evaporate during the process, leaving the dry stretched solid polymer on the metal collector. The jet flow towards the collector resembles spiraling motion rather than a straight path (3). In Bending instability of electrically charged liquid jets of polymer solutions in electrospinning by Reneker et al., the path is described to have 3 main stages, which are quoted below:

"Step 1 A smooth segment that was straight or slightly curved suddenly developed an array of bends.

"Step 2 The segment of the jet in each bend elongated and the array of bends became a series of spiraling loops with growing diameters.

"Step 3 As the perimeter of the loops increased, the cross-sectional diameter of the jet forming the loop grew smaller; the conditions for step 1 were established on a smaller scale, and the next cycle of bending instability began." (6)

The jet will keep spiraling towards the collector while forming new instabilities within itself (6). The overall flight path resembles a fractal pattern, which is determined by any pattern that defines its shape at any scale. Because of the flight path's instability and its complexity to predict using mathematical models, the fiber thickness on the metal collector varies almost randomly rather than a straightforward radial pattern.

Though operations of electrospinning are simple, and the learning periods for most researchers are brief, different combinations of parameters need to be explored so that the consistency of fiber formation is a guarantee. The different parameters and their impacts on fiber size, morphology and other overall quality have been extensively documented in various literature. In the article Effect of Electrospinning parameters on the Nanofiber Diameter and Length, by V. Beachley et al., the authors investigated the impacts of feed rate, polymer concentration, voltage, addition of salt, and plate size. Different parameters were experimentally explored, and the fibers' lengths and diameter information was collected and analyzed through Holm's test (7). Polymer solution flow rate seems to have minimal effects on the fiber quality. Although sufficient rate of feed is need for Taylor Cone formation, excess feed will merely accumulate on the needle tip or deposit on the collector in the forms of clumps or droplets (7). Solution concentration affects fiber

diameter and length with noticeable influences from small changes in concentration (7). Higher voltage also seemly has a positive impact on uniformity, but the system will produce fibers in short lengths (7). Collect plate size also changes the size of the ground terminal, therefore, changing product's diameter and length (7).

Enough distance allows the polymer solution to be sufficiently dried and stretched before reaching the grounded collector (8). Shorter distance also provides stronger electric field, which is also known to produce inconsistent results with increasing field strength (3), (7). Excessive distance makes sustaining an adequate and consistent electric field harder. It also allows more travel distance for the solution droplet, during which numerous flow instability can develop and cause inconsistent fiber thickness as well as possible excess beading. Bioresorbable Nanofiber-Based Systems for Wound Healing and Drug Delivery: Optimization of Fabrication Parameters by Katti et al. looks more in depth into the effect. It argued that it is rather the electric field strength density, represented by field strength in kilovolts per unit distance between the collector and the tip, that is important for product morphology change (9). A lower voltage or a longer collector distance can create weak electric field for polymer elongation. It is a more reasonable approach because the field strength is usually defined by both parameters. In their experiment, electric fields ranging from 0.5 to 1.5 kV/cm are tested for electrospinning (9). Their experimental data are presented in Figure 3. Through the results, they concluded that weak electric field can create thicker or even micron-sized fibers, and while higher voltage is generally favorable, excessively strong electric field can also have an adverse effect on fiber diameter (9). Therefore, it is important to experimentally explore the optimal electric field strength for each polymer and solvent combination.

Other environmental factors that are harder to control, such as humidity and temperature also have different degrees of effects on overall product outcome.

Because of its ease of production and overall versatility, nanofibers have been used in numerous applications, especially in medical applications and research. Drug and gene delivery with nanofibers has shown great promises due to the fibers convenience to include additional

formulations. Drugs can be simply mixed into the polymer solution and spun just as a part of fiber materials. The release mechanism can also be tuned from different geometrical designs to achieve release profiles from rapid to delayed (10). Hollow and core-shell fiber configurations can also be achieved by embedding a capillary inside the spinneret needle and feeding two immiscible solvents into the electrical field (11). Core-shell configuration specifically avoids the initial fast release of the loaded products and allows drug loading in the inner core of the product, thus permitting better tuning of the release profile through adjusting the thicknesses of the core and the shell.

When the formulation is chemically stable under electrospinning conditions, it can be embedded within the nanofibers through simple mixing with the spinning solution, the core-shell nanofibers can also be used to control the drug release profile. However, for unstable formulations, surface modifications are often done to the nanofibers to allow desired functionality after the nanofibers are already produced. In a review article by Hyuk Sang Yoo et al., three other common modification methods are introduced. Certain formulations and drugs cannot be blended into polymer solution for various reasons. Some hydrophilic drugs, such as chitosan, can be difficult to dissolve in polymer solvents such as chloroform. Furthermore, formulations containing nucleic acids or proteins can be

degraded when exposed to organic solvents, as well as, strong electric fields (12). The three common physical surface modifications are physical adsorption, surface nanoparticle adsorption, and layer-by-layer (LbL) layout (12). The illustration of the three modifications are shown in Figure 2 (12). Surface nanoparticle absorption allows nanoparticle integration into the fiber mesh. The particles can contribute a whole new spectrum of functionalities to the system, including secondary drug delivery, bactericidal properties and toxin neutralization. Chul Ho Park et al. combines the traditional electrospinning and electrospray methods and attaches nanoparticles onto the fiber surface through opposite electric charge attraction (13). Nanoparticles are sprayed through a separate nozzle charged with the opposite potential as the fiber electrospinning nozzle (13). In their experiment, NaF nanospheres are deposited onto the PMMA nanofiber surface (13). This modification adds another function to the nanofibers in dental applications as Fluorine can offer various dental benefits including resisting dental caries and demineralization (13), (14). Rujitanaroj et al. combines Ag nanoparticles with electrospun gelatin nanofibers (15). While gelatin nanofibers promote tissue growth, the silver nanoparticles give them an extra boost with offering antibacterial abilities (15).

Drug delivery applications with nanofibers have long been studied in the research and applied in medical fields. Wound healing capabilities of the nanofibers have also acquired increasing interests in research. Nanofibers not only promote tissue regrowth by mimicking the extracellular matrix but also allow loading of formulations such as curcumin and growth factors to further promote wound closure. Wound healing mechanisms and fiber assisted wound closure will be covered in greater details in the next chapter.

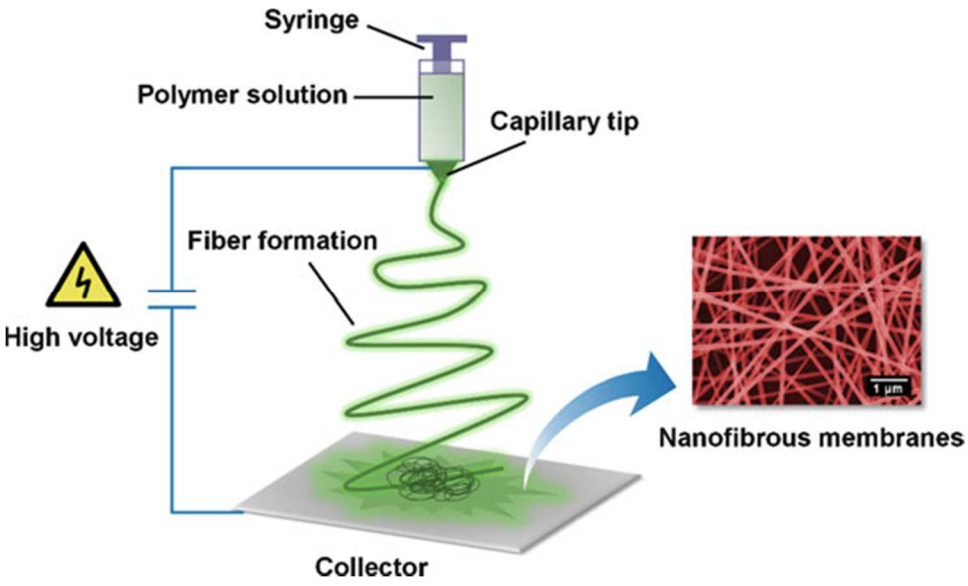

Figure 1 (3) Schematic illustration of a typical electrospinning setup

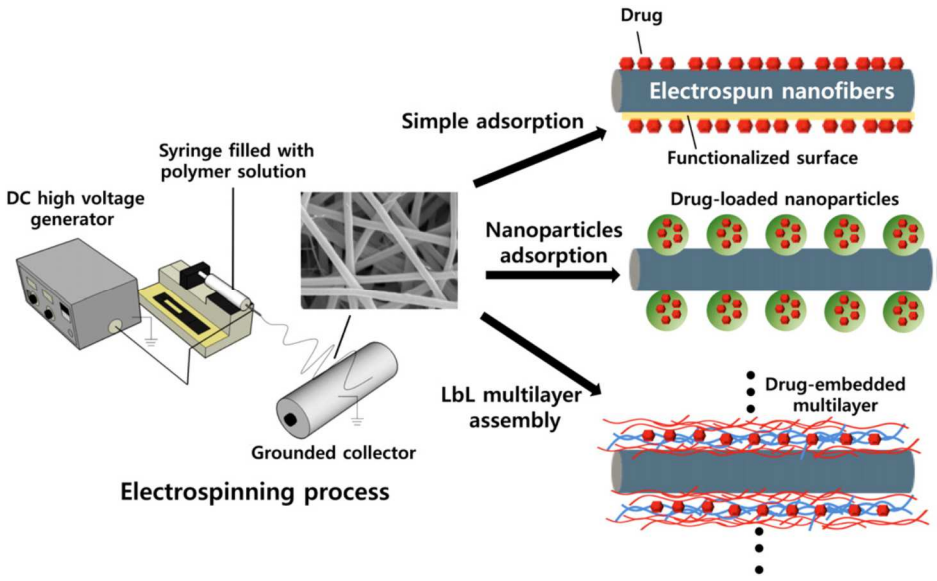

Figure 2 (12) the nanofiber fiber surface can be modified in several ways including simple drug adsorption, nanoparticle adsorption, and multilayer assembly

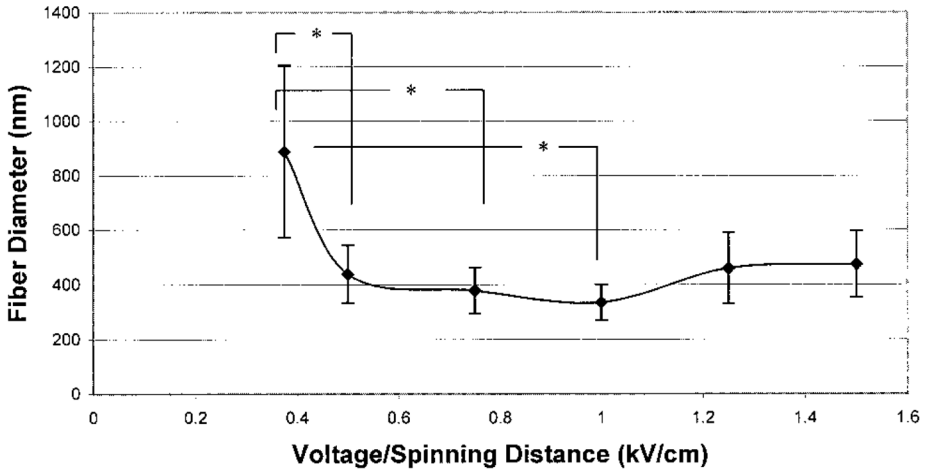

Figure 3 (9) The effect of voltage strength on resulting fiber diameter.

Nanofiber References

1. Zhou, Feng-Lei; Gong, Rong-Hua (2008). "Manufacturing technologies of polymeric nanofibres and nanofibre yarns". Polymer International. 57 (6): 837–845. doi:10.1002/pi.2395. ISSN 0959-8103.

2. Electrospinning and Nanofibers Advantages http://electrospintech.com/espinadvantage.html#.WS2kYmjysuV (accessed May 30, 2017).

3. Ding, B.; Yu, J. Electrospun Nanofibers for Energy and Environmental Applications; Springer Berlin Heidelberg: Berlin, Heidelberg, 2014.

4. Electrospinning of nanofibers: reinventing the wheel? Adv Mater

5. Structure and properties of keratin/PEO blend nanofibres

6. Reneker DH, Yarin AL, Fong H, Koombhongse S (2000) Bending instability of electrically charged liquid jets of polymer solutions in electrospinning.

7. Beachley, V.; Wen, X. Materials Science and Engineering: C 2009, 29 (3), 663–668.

8. Bhardwaj, N.; Kundu, S. C. Biotechnology Advances 2010, 28 (3), 325–347.

9. Katti, Dhirendra S., Kyle W. Robinson, Frank K. Ko, and Cato T. Laurencin. "Bioresorbable nanofiber-based systems for wound healing and drug delivery: Optimization of fabrication parameters." Journal of Biomedical Materials Research 70B.2 (2004): 286-96. Web.

10. Huang, Z.-M.; Zhang, Y.-Z.; Kotaki, M.; Ramakrishna, S. Composites Science and Technology2003, 63 (15), 2223–2253.

11. Li, D.; Xia, Y. Nano Letters 2004, 4 (5), 933–938.

12. Yoo, H. S.; Kim, T. G.; Park, T. G. Advanced Drug Delivery Reviews 2009, 61 (13), 1033–1042.

13. Park, C. H.; Kim, K.-H.; Lee, J.-C.; Lee, J. Polymer Bulletin 2008, 61 (4), 521–528.

14. Armstrong, W.d., and P.j. Brekhus. "Possible Relationship Between the Fluorine Content of Enamel and Resistance to Dental Caries." Journal of Dental Research 17.5 (1938): 393-99. Web

Curcumin

Derived from turmeric, curcumin has long been acknowledged as a healthful chemical due to its healing ability for the wound. It is derived from an Indian spice called Curcuma Longa Linn and used originally as a yellow food dye and food preservative (1). Curcumin was first purified from the spice in 1815 and its structure thoroughly studied by Kazimierz Kostanecki, J. Milobedzka and Kiktor Lampe in 1910 (2). The compound is fluorescent in acetonitrile $\lambda_{max} = 524$ nm, ethanol ($\lambda_{max} = 549$ nm), or micellar solution ($\lambda_{max} = 557$ nm) (3). It is soluble in most organic solvents and insoluble in water and many other common solvents such as ethanol (1). Curcumin is insoluble in water in acidic or neutral environments (< 0.1 mg/ml) but is more soluble in alkaline environments (3 mg/ml) (4).

Before it moved under the spotlight in research field, different turmeric curcumin supplements have already emerged in the consumer market and becoming more popular throughout the years because of its proclaimed health benefits in various traditions (5). In fact, in Indian Ayurvedic medicine turmeric has been used to treat all ranges of conditions and illnesses including wound, skin problems, and liver problems without any known side effects since 1900 BC (6), (7). Not only its benefits have been recognized through traditional practice but also scientific research has proven that curcumin has ability to interact with intracellular proteins and enzymes and influence signaling pathways (8). Curcumin targets multiple upstream pathways, many of which are unknown, to induce cell proliferation, reduce inflammation, and stop tumor growth.

Curcumin acts on multiple pathways to reduce the cells response to various pro-inflammatory cytokines. Many intracellular proteins can be mediated by curcumin at multitudinous levels and pathways. Nuclear factor κB (NF-κB), for example, is a major transcription factor protein responsible for the transcription of numerous pro-inflammatory cytokines, including tumor necrosis factor alpha (TNF-α), and interleukin-6 (IL-6), upon endotoxin or cytokine stimulation.

NF-κB is a heterodimer consisting of two subunits: RelA (p65) and NF-κB1 (p50) (9). With no stimulation, NF-κB is inhibited by the endogenous inhibitor IκB (9). Cytokines and endotoxins bind to their corresponding receptors on the cell membrane (for instance, TNF-α binds to TNFR receptor, and lipopolysaccharide (LPS) binds to Toll-like receptor4 (TLR4)) and undergo complex but similar pathways to activate NF-κB as the result. In the case of LPS/TLR4 interaction, it involves complicated interactions among membrane proteins such as TLR4, CD14, MD-2, and LPS binding protein (LBP) (10). In fact, LPS itself does not directly bind to the TLR4 receptor, according to Lu et al (10). LPS will bind directly to MD-2, a protein that attached non-covalently to TLR4 (10). The interaction can still happen without the presence of TLR4 in vitro, although TLR4 does increase the affinity of LPS to MD-2 (10). LBP, which is also known as the LPS shuttle protein, mediates the interaction of LPS with CD-14, which later helps transferring LPS to the TLR4/MD-2 receptor (10). Cytokines such as TNF-α and IL-6 undergo similar recognition processes though they involve different cytokine specific receptors. Upon accepting cytokine or endotoxin signals, protein NF-κB inhibiting kinase (NIK) is activated (9). NIK activates the IκB kinase complex (IKK), which is responsible for IκB phosporylation and ubiquination (9). IKK phosphorylates IκBα and IκBβ at serine residues

32 and 36, and residues 19 and 23, respectively (11). Then, IκB becomes phosphorylated and undergoes proteasome-mediated degradation through activation of 26S proteolytic complex (9), (12). Free NF-κB is therefore released to enable cytokine transcription (12). A detailed graphical demonstration of the activation in the cases of TNF-α and LPS stimulation is shown in Figure 4 (13).

Curcumin has been shown to reduce RelA (p65) nuclear translocation, IκBα degradation, and IκB serine 32 phosphorylation, according to Jobin et al (9). They conducted experiments to show decreased p65 translocation under IL-1β after curcumin treatment (9). In their study, HT-29 cells were first pre-treated with different doses of curcumin then stimulated with IL-1β (9). Nuclear extracts were taken from the cells and stained for p65 (9). Results are attached in Figure 5 (9). P65 translocation was not observed on the control cells (no IL-1β), but it was present upon cytokine stimulation (9). 75μM curcumin was enough to reduce p65 levels dramatically, as shown in the qualitative staining (9). A higher dose of curcumin of 150 μM decreased the levels even more (9). Meanwhile, p50, the other NF-κB subunit, remained unaffected (9). Jobin et al concludes that p65 is the major component inhibited by curcumin (9). The same can be seen in Figure 5 B. Caco-2 cells were treated with curcumin then inflammation induced with IL-1β (9). RelA (p65) is stained with anti-RelA primary antibody to visualize its translocation (9). An increased optical signal from p65 is observed when the cells are treated with IL-1β, yet the signals are not seen in either the cytokine-negative control group or the group treated with both IL-1β and 100 μM curcumin (9).

The group also conducted experiments to show curcumin can not only affect NF-κB activation through inactivating p65 translocation, but also modulates upstream pathways to inhibit its activation (9). Mitogen-activated protein kinase kinase kinase 1 (MEKK-1), according to Jobin et al, is a protein kinase that can activate NF-κB and many other separate signaling pathways, including the c-jun N-terminal kinase (JNK), as the result of a cytokine stimulation (TNF-α and IL-1) (9). JNK belongs to a pathway that is separate from the NF-κB activation with identical activation origin (MEKK-1) (9). Curcumin's inhibitory effects were demonstrated by measuring the luciferase activity after being incubated with MEKK-1 and curcumin (9). NF-κB inhibitor MG-132 was also used to demonstrate the effect of NF-κB inhibition on luciferase activities (9). Three groups of HT-29 cells were incubated with IL-8 luciferase reporter gene (IL-8 LUC) vectors, MEKK-1 and IL-8 LUC vectors, and MEKK-1, IL-8 LUC, and MG-132 expression vectors, respectively (9). Their data are included as Figure 6 (9). As expected MG-132, which expects to inhibit NF-κB expression, reduced the IL-8 luciferase activity (Figure 6A) (9). Curcumin targets MEKK-1 signaling pathway from cytokines and achieved a similar effect as the NF-κB inhibitor (Figure 6C) (9). The data are not surprising as curcumin is known to reduce NF-κB DNA binding, but what was interesting was that it also seems to affect another side pathway resulted from cytokine/MEKK-1 stimulation (9). Instead of IL-8 LUC, the group transfected TPA-responsive element reporter gene (TRE-LUC) into HT-29 cells (9). TRE-LUC works by detecting the binding activity of the binding site 12-O-Tetradecanoylphorbol-13-acetate (TPA) on Activator Protein-1 (AP-1) (14). AP-1 is related to c-jun and c-fos from a MEKK-1 side pathway separate from NF-κB activation (15). Upon cytokine activation, TRE-LUC detected activity from the TPA-responsive

element (9). The activity cannot be inhibited by MG-132 due to the fact that it is from a separate pathway (Figure 6B) (9). However, curcumin treatment is able to also reduce the luciferase signal (Figure 6D) (9). From their data, the group was able to conclude that in addition to the inhibition of specific elements, like IκBα and p65 in the NF-κB pathway, it also targets upper stream signaling pathways before the signals from MEKK-1 start branching off into multiple pathways (9).

Not only does curcumin inhibit pro-inflammatory cytokine production through affecting the corresponding signaling pathways in multiple levels, including modulating specific cytokine transcribing proteins, it also has been found to boost wound healing efficacy in vivo.

Aside from its well-proven anti-inflammatory efficacy, which promotes wound healing, curcumin helps wound closure at other stages as well. According to Akbik et al., fibroblast granulation tissue formation is essential for effective wound healing, as some chronic wound failed to heal due to inhibitions of fibroblast migration and granulation (16). Mohanty et al. developed a type of curcumin loaded Oleic Acid Based Polymeric (COP) bandage to accelerate wound healing (17). Although the material itself is expected to provide some wound healing benefits, curcumin further enhances the efficacy of the whole system (17). In their in vivo study, their bare polymeric bandage without curcumin showed moderate wound healing efficacy compared to the control group (17). However, when the material is loaded with curcumin, wound closure was accelerated even further, with the wound closing almost completely on the Day 10 (17). Furthermore, myofibroblast staining using smooth muscle α actin (SMA) also showed increased myofibroblast distribution on

the wound of curcumin treated group, superseding both the control and blank bandage groups (17). The result suggests that curcumin enhances wound closure by promoting fibroblasts/myofibroblasts proliferation at the wound site.

In addition, curcumin has been shown to improve collage deposition as well, according to Akbik et al. (16). Described in the wound healing section, collage deposition is the last extracellular matrix formation during wound healing. Curcumin is able to help produce thicker and compact collage extracellular matrix, according to Dai et al (18). From their Masson's Trichrome staining for collagen, their group of mice treated with curcumin loaded chitosan alginate sponge was able to produce well-aligned collagen matrix, and it is thicker than both the control group (gauze only), and the bare alginate sponge groups (18).

Cell apoptosis is also important because the wound needs to be rid of extra inflammatory cells in order to progress from the inflammatory phase to proliferation phase (16). Using agarose gel electrophoresis, Mohanty et al. detected higher levels of apoptotic cells in their COP and bare bandage groups compared to control on Day 4, with COP treated mice presenting slightly higher apoptotic levels (17). On Day 10, COP group had decreased levels of apoptosis, indicating the wound moving out of the inflammation stage, whereas the control and bare bandage groups showed higher levels apoptosis (17).

Even though curcumin promises impressive in vitro and in vivo efficacy, its physical properties can dramatically limit the drugs in vivo bioavailability. Other sources have suggested that the drug degrades quickly under neutral or alkaline conditions but is

stable in pH < 6.0 (4). Thus, its poor solubility in stable pH and many other properties limit curcumin's bioavailability, and it's mostly widely applied in tubular lower GI tract (4).

A chemical compound's Bioavailability can be determined by its many properties and interactions with a physiological system. For example, a drug's poor bioavailability can be caused by its low rates of uptake and metabolism, fast clearance from the body, and low intrinsic activity etc. (6) In the case of curcumin, problems such as short half-life, fast metabolism, low serum levels and tissue distribution negatively impacted curcumin's bioavailability (6). According to Anand et al., curcumin's bioavailability is limited through four major aspects: low serum concentration, poor tissue distribution, fast clearance, and short half-life (6).

Low curcumin serum level was observed by Wahlstrom et al. through monitoring blood plasma curcumin levels after orally administering 1g/kg of curcumin to rats (19). Negligible amount of curcumin was detected in the plasma (19). When the dosage is increased to 2g/kg to rats, curcumin serum concentration is detected at 1.35 μg/ml after 0.83h (20). However, when humans are exposed to the same dosage the serum level can be low or undetectable (20). Curcumin serum levels can be boosted by injecting the drug intravenously (i.v.). Same dosage of 10 mg/kg to rats showed a six-fold increase when introduced i.v. versus orally (21).

Low serum concentration naturally leads to low tissue distribution. After oral administration of curcumin, 90% of curcumin stayed in the stomach after 30 mins, and 1% left after 24 hours, according to Ravindranath et al (6), (22). Through measuring tritium-labeled curcumin levels in the tissue after oral administration, 400 mg curcumin intake

yielded a significant amount of radio-labeled curcumin signals (23). However, more curcumin intake did not increase the levels, indicating the maximum tissue absorption is extremely low (23). The adsorption levels stopped following a dose-dependent trend at very low levels of curcumin intake. In the case C57B1/6J mice, when they were fed with 0.2% curcumin diet for one week, then curcumin was withdrawal from the diet, their tissue curcumin levels decreased to undetectable levels after just six hours (6). i.p. injection also showed little success in curcumin tissue retention. According to Perkins et al, C-14 labeled curcumin was injected through i.p. and the curcumin tissue levels are monitored (24). Liver, kidneys, and intestinal mucosa showed the highest peak concentrations of curcumin after injection, while there were detectable nmol/g levels of drug uptake in the brain, heart, lungs, and muscles, but the drug levels in all those organs quickly dropped to 20-33% of the original concentration after only 4-8 hours (24).

Another reason for curcumin's poor bioavailability is high metabolism in the body. Major metabolites such as glucuronides of tetrahydrocurcumin (THC) and hexahydrocurcumin (HHC) are identified in rates (6). Asai et al concluded that major curcumin glucuronidation enzymatic activities in the kidneys and digestive tracts may result in blood being exposed to mainly metabolized curcumin (25).

Curcumin's poor bioavailability shown through poor serum concentrations, tissue distribution and presence of major metabolites greatly limit its clinical application and efficacy. Therefore, researchers have considered numerous delivery platforms, including the nanofibers, to maximize the bioavailability of the drug.

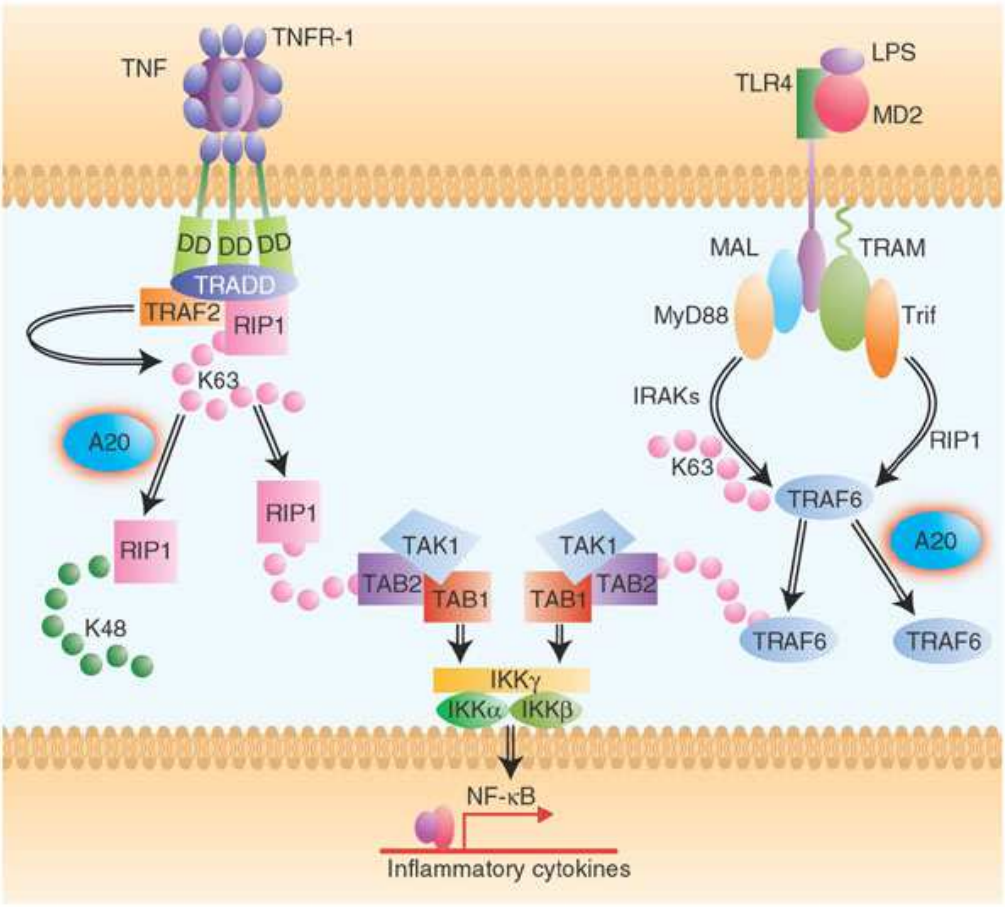

Figure 4 (13) schematic illustration of signaling pathways of LPS and cytokines (TNF-α). NF-κB is activated as the result of both events.

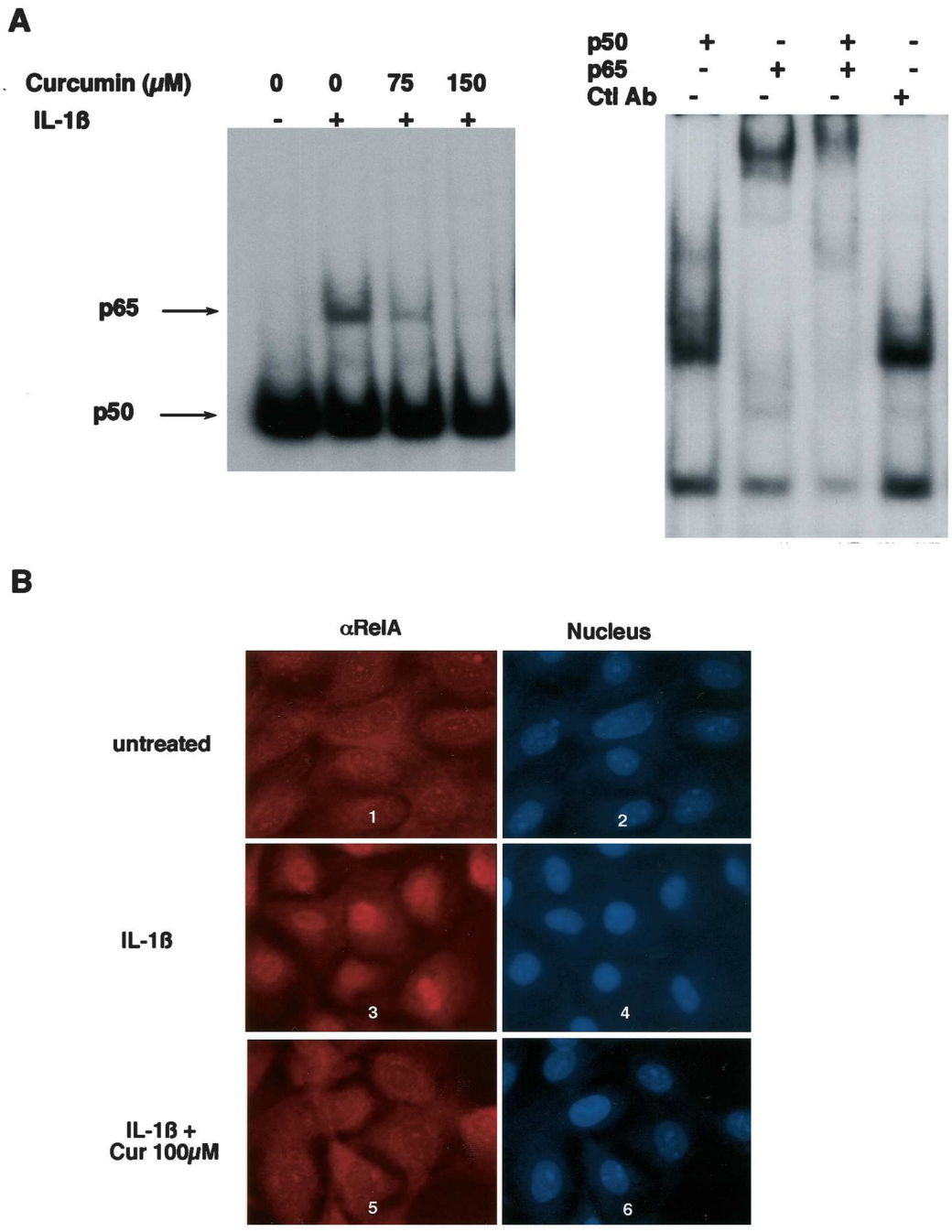

Figure 5 (9) p65 (RelA) is the main dimer of NF-κB inhibited by curcumin

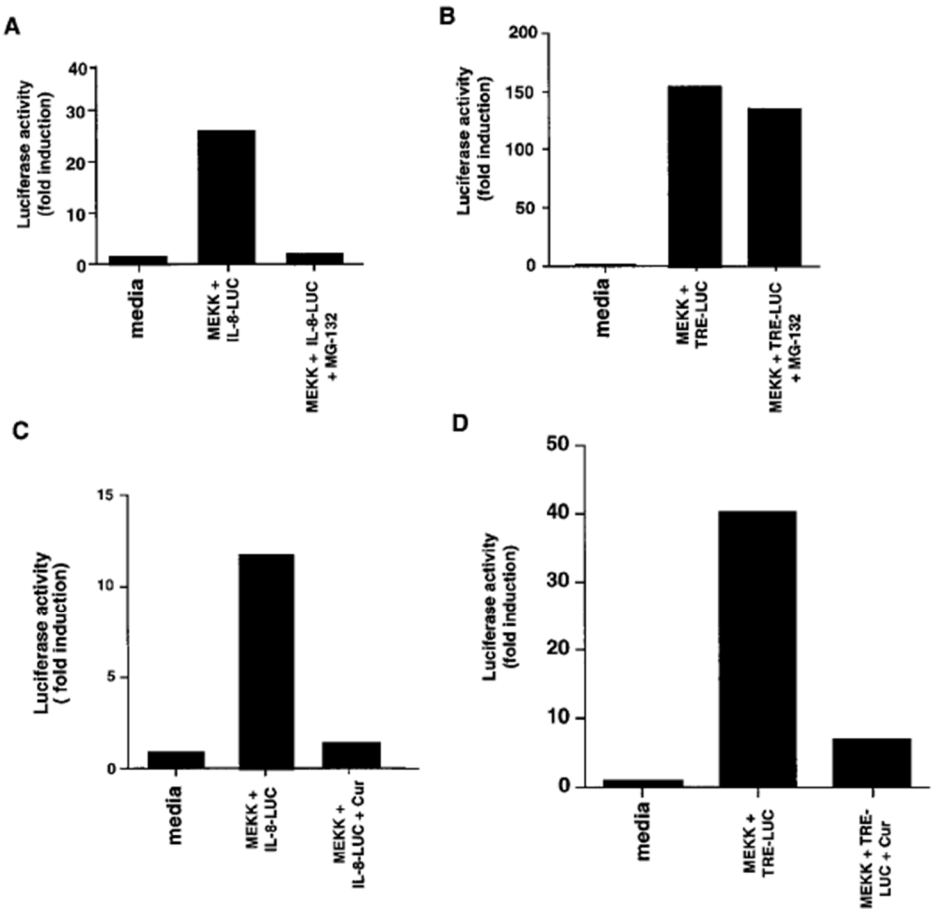

Figure 6 (9) IL-8 luciferase activity after MEKK-1 stimulation is inhibited by curcumin. IL-8 luciferase is associated with NF-κB pathway activation. At the same time TPA-responsive element activity is associated with NF-κB but it is still modulated by curcumin.

Curcumin References

1. Allegra, A.; Innao, V.; Russo, S.; Gerace, D.; Alonci, A.; Musolino, C. Cancer Investigation 2016, 35 (1), 1–22.

2. Ravichandran, R. Advances in Nanoparticles 2013, 02 (01), 51–59.

3. Chignell, C. F.; Bilskj, P.; Reszka, K. J.; Motten, A. G.; Sik, R. H.; Dahl, T. A. Photochemistry and Photobiology 1994, 59 (3), 295–302.

4. Ravichandran, R. "Studies on Dissolution Behaviour of Nanoparticulate Curcumin Formulation." Advances in Nanoparticles 02.01 (2013): 51-59. Web.

5. History of curcumin http://www.curcuminforhealth.com/history/ (accessed Mar 19, 2017).

6. Anand, P.; Kunnumakkara, A. B.; Newman, R. A.; Aggarwal, B. B. Molecular Pharmaceutics2007, 4 (6), 807–818.

7. Ammon, H.; Wahl, M. Planta Medica 1991, 57 (01), 1–7.

8. Zingg, J.-M.; Meydani, M. BioFactors 2012, 39 (1), 1–1.

9. Jobin, C; Bradham, C; Russo, M; Juma, B; Marula, A; Brenner, D; Sartor, R. J Immunol 1999; 163:3474-3483;

10. Lu, Y., Yeh, W., & Ohashi, P. S. (2008). LPS/TLR4 signal transduction pathway. Cytokine, 42(2), 145-151. doi:10.1016/j.cyto.2008.01.006

11. Mercurio, F. (1997). IKK-1 and IKK-2: Cytokine-Activated IB Kinases Essential for NF-B Activation. Science, 278(5339), 860-866. doi:10.1126/science.278.5339.860

12. Stancovski, I., and D. Baltimore. 1997. NF-kB activation: the IkB kinase revealed? Cell 91:299.

13. Silverman, N., & Fitzgerald, K. (2004). DUBbing down innate immunity. Nature Immunology,5(10), 1010-1012. doi:10.1038/ni1004-1010

14. Angel, Peter, Masayoshi Imagawa, Robert Chiu, Bernd Stein, Richard J. Imbra, Hans J. Rahmsdorf, Carsten Jonat, Peter Herrlich, and Michael Karin. "Phorbol ester-inducible genes contain a common cis element recognized by a TPA-modulated trans-acting factor." Cell 49.6 (1987): 729-39. Web.

15. Rauscher, F. J., P. J. Voulalas, B. R. Franza, and T. Curran. "Fos and Jun bind cooperatively to the AP-1 site: reconstitution in vitro." Genes & Development 2.12b (1988): 1687-699. Web.

16. Akbik, D.; Ghadiri, M.; Chrzanowski, W.; Rohanizadeh, R. Life Sciences2014, 116 (1), 1–7.

17. Mohanty, C.; Das, M.; Sahoo, S. K. Molecular Pharmaceutics 2012, 9 (10), 2801–2811.

18. Dai, Mei, Xiuling Zheng, Xu Xu, Xiangye Kong, Xingyi Li, Gang Guo, Feng Luo, Xia Zhao, Yu Quan Wei, and Zhiyong Qian. "Chitosan-Alginate Sponge: Preparation and Application in Curcumin Delivery for Dermal Wound Healing in Rat." Journal of Biomedicine and Biotechnology 2009 (2009): 1-8. Web.

19. Wahlström, Bo, and G. Blennow. "A Study on the Fate of Curcumin in the Rat." Acta Pharmacologica et Toxicologica 43.2 (2009): 86-92. Web.

20. Shoba, Guido, David Joy, Thangam Joseph, M. Majeed, R. Rajendran, and P. Srinivas. "Influence of Piperine on the Pharmacokinetics of Curcumin in

21. Yang, Kuo-Yi, Lei-Chwen Lin, Ting-Yu Tseng, Shau-Chun Wang, and Tung-Hu Tsai. "Oral bioavailability of curcumin in rat and the herbal analysis from Curcuma longa by LC–MS/MS." Journal of Chromatography B 853.1-2 (2007): 183-89. Web.

22. Ravindranath, Vijayalakshmi, and Nanjundiah Chandrasekhara. "Absorption and tissue distribution of curcumin in rats." Toxicology 16.3 (1980): 259-65. Web.

23. Ravindranath, Vijayalaksmi, and Nanajundiah Chandrasekhara. "Metabolism of curcumn-studies with [3H]curcumin." Toxicology 22.4 (1981): 337-44. Web.

24. Perkins, S; Verschoyle, R. D.; Hill, K.; Parveen, I.; Threadgill, M. D.; Sharma, R. A.; Williams, M. L.; Steward, W. P.; Gescher, A. J. Chemopreventive efficacy and pharmacokinetics of curcumin in the min/+ mouse, a model of familial adenomatous polyposis. Cancer Epidemiol. Biomarkers PreV. 2002, 11 (6), 535–40 .

25. Asai, Akira, and Teruo Miyazawa. "Occurrence of orally administered curcuminoid as glucuronide and glucuronide/sulfate conjugates in rat plasma." Life Sciences 67.23 (2000): 2785-793. Web.

Wound Healing

Wound healing is one of the primary areas of focus in nanotechnology. Nanotechonogy enables ease in delivering wound healing promoting formulations. Nanoparticles, such as silver particles can be used to as an effective anti-microbial agent. Due to the small size of the nanoparticles and their surface area to weight ratio, nanoscale reaction and bactericidal activities are enhanced (1). Curcumin loaded nanoparticles are widely researched for wound healing. The ingredient itself not only has anti-bacterial abilities, but also anti-inflammatory and anti-tumor activities. The functions of curcumin and its anti-inflammatory is discussed in Curcumin Chapter.

Wound healing is an extremely complicated mechanism and involves the interactions from many immune cells, pro-inflammatory cytokines, growth factor, and different types of extracellular matrices. Cutaneous Wound Healing by Singer et al. discusses in great details of the wound healing mechanism. According to the article, when a tissue is damaged, it undergoes complicated mechanisms including inflammation, epithelialization, granulation tissue formation, neovascularization, and wound contraction (2). Blood clots in forms of extracellular matrix, which favors cell migration (2). Infiltrations of neutrophils, monocytes, and macrophages fight against infection and start inflammation (2).

Neutrophils migrate to wound site within the first 48 hours (3). Macrophage infiltration starts to dominate after 3 days while neutrophil count at wound begins to decrease (3). During the process of inflammation, many inflammatory cytokines, including tumor necrosis factor α (TNF-α), interleukin-1 beta (IL-1β), interleukin-2 (IL-2), and interleukin-6 (IL-6). Cytokines, such as interleukin-1 (IL-1), are especially important since

it prepares the wound for neutrophil migration, which is the immune system's first step of defense mechanism (4). The production of different growth factors in keratinocytes and fibroblasts, including the vascular endothelial growth factor (VEGF), can be stimulated by the secretion of cytokines such as TNF-α and IL-1β (4). VEGF-A binds to two surface receptor tyrosine kinases KDR and Flt-1 (4), (5). In vitro, once bound to VEGF, KDR increases cell proliferation and survival (5). VEGF bound Flt-1 is responsible for chemotaxis and controlling vascular permeability (4), (5). Through comparing with the wound closure of macrophage depleted mice, it has also been experimentally proven that growth factor productions are crucial to wound healing (2).

Although normal inflammation can benefit wound closure by promoting immune cell recruitment through cytokine production and cell immigration and proliferation through growth factor secretion, other sources suggest excessive inflammation can be counterproductive to wound healing. In Factors Affecting Wound Healing by Guo et al., the group proposed the concept of detrimental effect of prolonged pro-inflammatory cytokine exposure to the wound (6). Bacteria and endotoxins can force the wound to go into chronic inflammation phase where cytokines such as TNF-α are expressed for an extended period (6). This can increase the levels of matrix metalloproteases (MMPs) at wound site, which can cause excessive extracellular matrix degradation (6). High protease content can also mean growth factors may also be degraded at wound site (6).

Additionally, while neutrophils clean the wound and help fight infection, they do not seem to contribute directly to the wound healing process. Excessive neutrophil activation can cause unnecessary elevation of pro-inflammatory cytokines and reduced production of growth factors (7). In Inflammation and Wound Healing by Tatiana

Oberyszyn, the review article suggested that research has been done to deplete neutrophils in lab animals (8). While the wound healing had to be kept sterile to prevent infection, neutrophil depleted mice had more accelerated wound closure than normal mice, suggesting while neutrophil infiltration and inflammation can have adverse effect on wound closure (8), (9). Martin et al. investigate on the mechanism further and observe intact the wound healing process in PU.1 knockout mice (10). PU.1 null mice are depleted of both neutrophils and macrophages. Scaring is significantly reduced after neutrophil and macrophage depletion (10). Inflammatory cytokines such as IL-6 are absent due to the absence of immune cells, but crucial growth factor TGF-β is not missing in PU.1 null mice, though the growth factor levels are reduced due to macrophage absence (10). The fact PU.1 null mice healed without scarring may have suggested that excessive cytokine and growth factor production might be the reason for unnecessary "matrix deposition and scar contracture post-repair", according to Martin et al. (10).

Other than immune cell infiltration and inflammatory cytokine and growth factor production, cell epithelialization also happens rapidly after a wound is created. Inter-cellular links, such as hemidesmosomal, between dermal and epidermal cells are broken down to allow movement of the cells along the extracellular matrix (2). Epidermal cells possess integrin receptors on membrane to attach and adhere to extracellular matrix proteins from the blood clot (2). At the same time, the production of collagenase and plasmin are stimulated by epidermal cells to degrade the extracellular matrix made by blood clot, which is later replaced by fibroblast extracellular matrix (2), (11). After the epidermal cells start to degrade the extracellular matrix from blood clot, fibroblasts cells in the form of granulation tissues move into the wound site (2). The cells start producing

collagen and replace the existing extracellular matrix with collagenous matrix (2). After collagen is sufficient to cover wound area, the fibroblasts stop collagen production and undergo apoptosis (2). Unwanted activation of neutrophils can over-produce enzymes that can break down tissues at wound site, leading to even more neutrophil recruitment, a positive feedback loop (7). As a result, granulation tissue re-formation stage of wound healing can be severely hindered due to the fact that the new collage extracellular matrix will also be broken down.

Due to their unique structure and thin diameter, nanofibers become increasing desirable wound closure treatment. They can mimic the extracellular matrix in the blood clot as well as the collagen stages, which support cell migration and proliferation in wound healing. In addition to their inherent ability to promote wound healing, different drugs and formulations can be loaded into the fiber membrane to further ease wound healing process. Many groups have successfully loaded surfactants into polymer nanofibers to modify the fibers' hydrophobicity, which can enhance cell adhesion. Growth factors have also been coated on the cell surface to mimic growth factor secretion from the macrophage cells.

On Sook Hee Ku et al., the group separately coated gelatin and poly (dopamine) (PDA) onto polycaprolactone (PCL) fibers in the effort to promote cell growth. They first start by observing the change in hydrophobicity by measuring the static contact angle when a drop of water rests on the surface to each fiber sample (12). The PCL fibers themselves are extremely hydrophobic, resulting in larger contact angles with the water droplet. The angles for PCL fibers and PCL homogenous film are $92.^{\circ}$ and 83°, respectively (12). When the nanofibers are coated with gelatin or PDA, they become hydrophilic and,

consequently, absorb water immediately onto their surface, minimizing the contact angle to zero (12).

Human umbilical vein endothelial cells (HUVECs) are also cultured on the sample surfaces to investigate cell viability and proliferation (12). Even though both gelatin and PDA-coated nanofibers increase the hydrophilicity of the fibers, HUVECs attach and proliferate a lot better on the latter. The cell morphology can be shown in Figure 10 A (12). Because of the hydrophobic nature of bare PCL fibers, fewer cells adhered on the nanofibers, and for those that are attached, less area is occupied by each cell on the fiber surface (12). Cell count revealed that there is little difference between gelatin-coated and bare PCL nanofibers, whereas PDA-coated fibers acquired a significantly larger number of cells (Fig. 3.4B) (12). Cell viability (MTT) assay also showed a dramatic boost of cell viability in the PDA-coated nanofibers sample compared to bare PCL fibers (Fig. 3.4C) (12). One can conclude from their results that nanofibers not only provide a perfect platform for cell adhesion and growth, but also allow a platform to include more cell adhesion promoting materials, which further increase cell viability and proliferation.

Other than coating growth factors and pro-adhesion materials on the nanofiber surface, the fibers can also be used to act as a drug delivery platform to deliver and control the release of anti-bacterial, anti-cancer, or anti-inflammatory drugs. Nguyen et al investigated the wound healing efficacy of curcumin-loaded poly lactic acid (PLA) nanofibers (13). The curcumin has long been researched and used as an effective anti-inflammatory and anti-tumor agent, but due to its poor solubility in water, the drug has limited bioavailability in free form (14). The group dissolved both curcumin and PLA into organic solvent (chloroform/DMAc) and spun the solution into nanofibers with diameters

560-970 nm (13). C2C12 mouse myoblast cells are cultured on the surface of the nanofibers at different curcumin loading (13). Cell viability assay reveals that PLA fibers have some negative impact on viability (Figure 9) (13). Though the effect is not significant, the group conclude it can be attributed to the fibers high hydrophobicity, a problem that can be easily amended by coating hydrophilic material on the surface as performed in Ku et al. (12), (13). While moderate curcumin loading does not seem to have major impact on viability, increasing the curcumin content shows decreasing trend in viability (13). Higher curcumin content (>25uM) can even be toxic to the cells (13). Cell attachment assay also showed very similar results (Figure 10) (13).

The group further investigated the in vivo wound healing efficacy (13). C57BL/6 mice were used to observe the effects of different treatments (13). Burned skin wound is created by pressing a 7mm disk to the back of the mice (13). The wounds are created by blank PLA fibers and curcumin loaded PLA fibers (13). The efficacy is observed over the period of 15 days, and the wound closure images are shown in Figure 11 (13) and the quantitative wound closure rate are presented in Figure 12 (13). According to the figures, even the blank PLA provided efficacy for wound healing (13). Mainly because PLA provides the same structure as the provisional and collage extracellular matrices. The great biocompatibility of PLA and the structure's porosity can also help cell attachment on the fiber membrane surface (13). But more importantly, according to Figure 12, though the differences are not as significant at the end of 15 days, curcumin fibers are the only group which completely close the wound (13). Additionally, curcumin fibers provided significant efficacy during the early stage of the healing trial (13). Despite of the small difference in the wound healing rate at the end of the trial period, through the pictures, the group also

concluded that the epithelialization stage of wound healing was almost done in the curcumin loaded fiber group within 7 days while the control group took over 15 days to complete the stage (13). Unfortunately, the group did not include further information about the healing process beyond day 15, but since the curcumin fiber group was at least 8 days ahead of the control group, large difference in total wound closure between the two groups can also be expected. As a side note, the group also discovered that the wounds from all mice in the curcumin group healed completely with relatively less scarring (13). This can be contributed to the fact that other than the anti-inflammatory effects of curcumin, it is also able to promote cell mobility and re-epithelialization at the early stage of wound healing because of its ability to induce hexosamine and uronic acid production (13), (15).

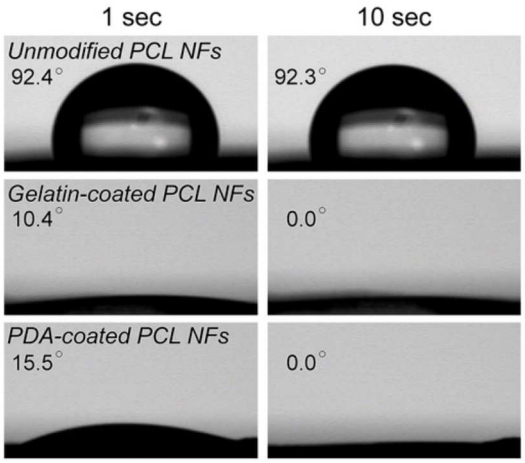

Figure 7 (12) surface modification of nanofibers changes the surface hydrophobicity and hence the contact angle with water

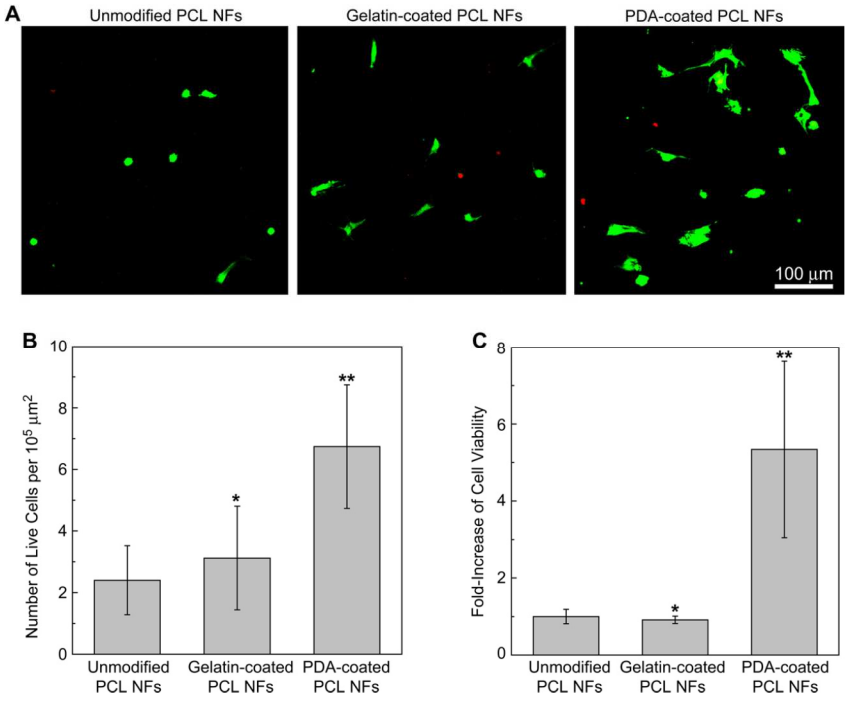

Figure 8 (12) surface modified nanofiber provides an excellent platform for cell proliferation.

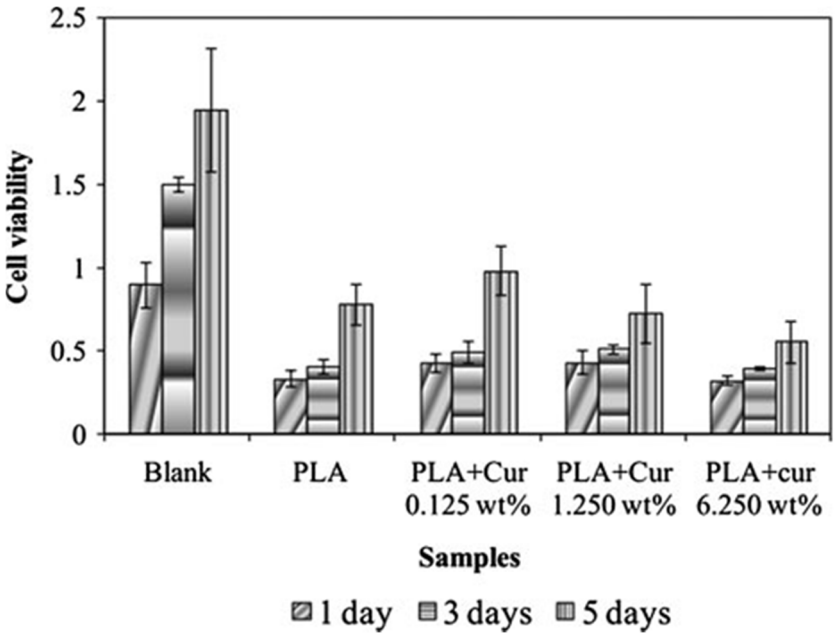

Figure 9 (13) hydrophobic surface of the nanofibers can negatively impact cell viability. Also, higher curcumin loading could decrease cell viability as well.

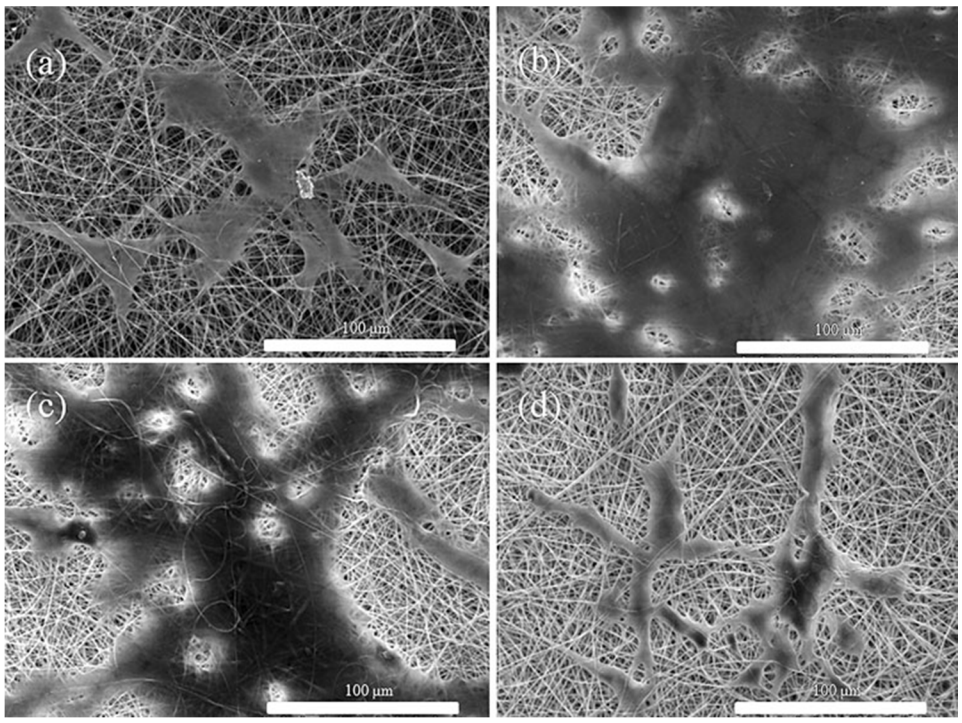

Figure 10 (13) higher curcumin content (>25 uM) can negatively impact cell proliferation

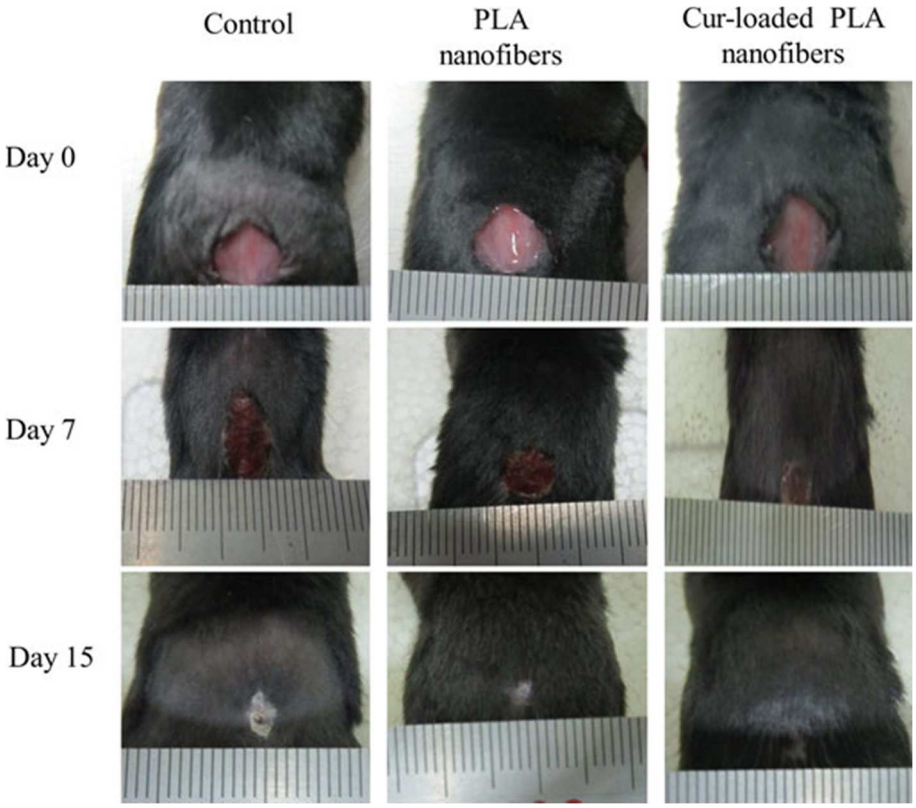

Figure 11 (13) PLA nanofibers can accelerate wound healing due to its ECM mimicking structure. Curcumin loaded PLA nanofibers can promote wound healing even further due to various anti-inflammatory effects of curcumin.

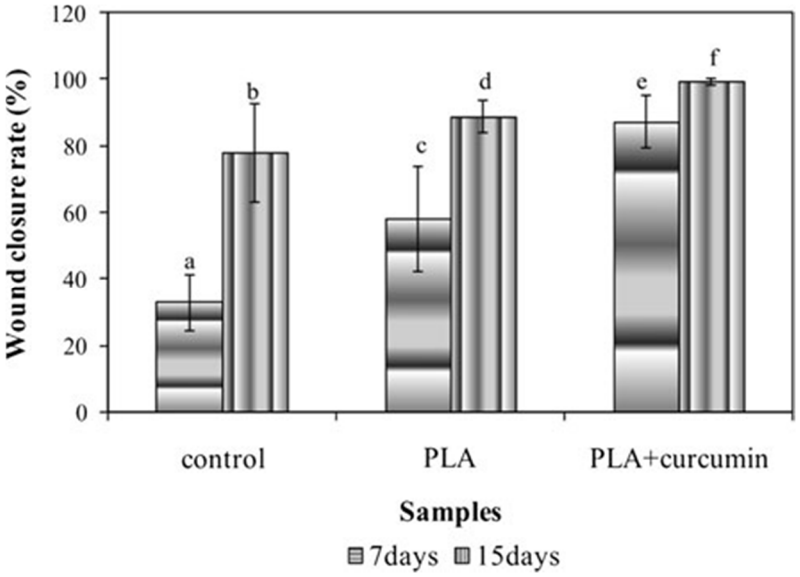

Figure 12 (13) wound closure rates from control (no treatment), PLA nanofibers, and curcumin loaded PLA nanofibers

Wound Healing References

1. "Nanotechnology accelerates wound healing." Dermatology Times. Advanstar Communications Inc, n.d. Web. 13 Feb. 2017.
2. Epstein, F. H.; Singer, A. J.; Clark, R. A. New England Journal of Medicine 1999, 341 (11), 738–746.
3. Leibovich SJ, Ross R. The role of the macrophage in wound repair: a study with hydrocortisone and antimacrophage serum. Am J Pathol 1975;78:71-100.
4. Barrientos, S.; Stojadinovic, O.; Golinko, M. S.; Brem, H.; Tomic-Canic, M. Wound Repair and Regeneration 2008, 16 (5), 585–601.
5. Wang, D. Journal of Biological Chemistry 2000, 275 (21), 15905–15911.
6. Guo, S.; Dipietro, L. A. Journal of Dental Research 2010, 89 (3), 219–229.
7. Menke, N. B.; Ward, K. R.; Witten, T. M.; Bonchev, D. G.; Diegelmann, R. F. Clinics in Dermatology 2007, 25 (1), 19–25.
8. Oberyszyn, T. M. Frontiers in Bioscience 2007, 12 (8-12), 2993.
9. Dovi, J. V. Journal of Leukocyte Biology 2003, 73 (4), 448–455.
10. Martin, P.; D'souza, D.; Martin, J.; Grose, R.; Cooper, L.; Maki, R.; Mckercher, S. R. Current Biology 2003, 13 (13), 1122–1128.
11. Pilcher, B. K.; Dumin, J. A.; Sudbeck, B. D.; Krane, S. M.; Welgus, H. G.; Parks, W. C. The Journal of Cell Biology 1997, 137 (6), 1445–1457.
12. Ku, S. H.; Park, C. B. Biomaterials 2010, 31 (36), 9431–9437.
13. Nguyen, Thuy Thi Thu, Chiranjit Ghosh, Seong-Gu Hwang, Lam Dai Tran, and Jun Seo Park. "Characteristics of curcumin-loaded poly (lactic acid) nanofibers for wound healing." Journal of Materials Science 48.20 (2013): 7125-133. Web.
14. Manju, S., and K. Sreenivasan. "Conjugation of curcumin onto hyaluronic acid enhances its aqueous solubility and stability." Journal of Colloid and Interface Science 359.1 (2011): 318-25. Web.
15. Panchatcharam, Manikandan, Sumitra Miriyala, Vinaya Subramani Gayathri, and Lonchin Suguna. "Curcumin improves wound healing by modulating collagen and decreasing reactive oxygen species." Molecular and Cellular Biochemistry 290.1-2 (2006): 87-96. Web.

Cell Membrane Coating and Nanofiber Attachment

Nanoparticle cell membrane coating technology was first developed by Dr. Liangfang Zhang in effort to produce a biomimetic system that improves in vivo circulation time while minimizing the traditional downsides of using conjugates. Before the emergence of membrane camouflaged nanoparticles, conjugation of polyethylene glycol (PEG) was used to solve most drugs poor circulation problems. PEG was first discovered by FF Davis et al in 1977 in his paper Alteration of Immunological Properties of Bovine Serum Albumin by Covalent Attachment of Polyethylene Glycol (1). The group modified a typical immunogenic protein, bovine serum albumin (BSA), by blocking the functional groups on the surface with nonimmunogenic polymer chains and made it nonimmunogenic (1). The size of the molecule also dramatically increased so that renal clearance is minimized (1). Because of PEG's simple production process and proven efficacy, it became one of the most widely used medium for improving in vivo circulation. Although PEGylation shows attractive efficacy, researchers gradually realized that certain key drawbacks prohibit the adoption of the technology. According to Fan Zhang et al., the nonimmunogenic promise of the conjugate is not full-proof; the benefits do not come without consequences (2). One of the main downfalls of using PEG is the concern over developing anti-PEG anti-body. According to Sroda et al., PEG will not remain nonimmunogenic for long if the a biological system is exposed to repeated doses (3). Repeated injection of PEG can trigger the immune response and stimulate the biological system to produce PEG antibodies (3). In their experiments, the detection of carboxyfluorescein (CF) was used to represent the immunoreactivity under PEG stimulation (3). Three groups of PEGylated liposomes were incubated with 10 mM HEPES

and 140 mM NaCl solution, serum from rabbits not exposed to PEG, and serum from animals that have been injected with PEG-liposomes for 7 consecutive days (3). The results from CF assay showed that CF intensity is the highest from the third group, with the first group being the lowest of that (3). This indicates presence of immune response to PEG-liposomes after repeated exposure.

Zhang et al used the structure of red blood cell membranes to cloak nanoparticles so that the immune system fails to recognize them as foreign objects. The body undergo phagocytosis when encountering foreign objects in the system (4). Phagocytes do not engulf non-foreign cells mainly because a marker CD47 is expressed on most cells (4). Tsai et al. conducted experiments comparing the phagocytosis activity with bare microbeads and those coated with CD47 (4). The result showed that the majority CD47 coated beads were able to avoid phagocytosis in both cases of human and mouse CD47's (4). Bioconjugation of CD47 has not been successful in preventing protein denaturization (5). Red blood cells are natural carriers in the body for oxygen delivery. Membrane coated nanoparticles are able to demonstrate an even longer circulation half-life than PEGylated nanoparticles while avoiding possible production of antibodies (5). Human and mouse red blood cells express CD47 on the membrane surface so the derived membranes preserve those markers and can camouflage biocompatible materials through membrane coating (6).

Membrane coating can offer benefits other than improving circulation in the system. Different cell membrane type can offer specific functions to achieve various clinical efficacies. For example, RBC generally are the most available and Dr. Liangfang Zhang's lab has done extensive research on RBC membrane coated particles. In the case of RBC

membrane coating, the nanoparticles are also able to neutralize a broad spectrum of pore-forming toxins (7). According to Zhang et al., RBC membrane coated poly(lactic-co-glycolic acid) (PLGA) nanoparticles are able to reduce or, in some cases, completely avoid lysis of red blood cells from most pore forming toxins, including α toxin (7). α-toxin lyses the red blood cells through anchoring its molecules on the cell surface (8). Molecules can link each other through non-covalent interactions and form pores that exposes intracellular fluid to outside environment, causing cell death (8). Those toxins can have similar or identical effects on RBC membrane coated nanoparticles but due to the nanoparticles' high surface area, attachment onto the nanoparticle surface can be more favorable than that of the cells in theory. In Figure 13a and b, through both qualitative and quantitative data, RBC nanoparticles are able to protect the cells from being lysed while all other formulations fail (7). Blotting (Figure 7d) also shows toxin binding on both RBC vesicle and RBC membrane coated particles (7).

Cell membrane coating technology can also be used for detoxifying chemical toxins such as organophosphates. According to Kroll et al., organophosphates, commonly seen as commercial pesticides, work by phosphorylating acetylcholinesterase (AChE), which is responsible for inhibiting the degradation of acetylcholine (ACh), a neurotransmitter (9). RBC membrane coating can reduce the toxic effects by allowing the chemical to attack the acetylcholinesterase provided by the cell membrane (9). The illustrations of the RBC membrane NPs' role in preventing dichlorvos (DDVP), a type of organophosphate, from inhibiting AChE and leading to accumulation of ACh in the synapse are shown in Figure 14 (10). Pang et al., mice was given lethal intravenous injection of DDVP (10 mg/kg) (10). Then, three different groups were given no treatment (PBS), PLGA-PEG NP and RBC NP,

respectively (10). The first two groups reached 100% death within 12 mins, whereas, RBC NP group had zero fatality (10). Orally administration (150 mg/kg) also showed similar results, with the RBC NP group being able to prevent any death by the organophosphate (10).

In addition to the use of RBC membrane for pore-forming toxin neutralization and organophosphates, other membranes are used to fit other purposes. For example, macrophage membranes have been used to neutralize cytokines and endotoxins (lipopolysaccharide (LPS)) (11). The functions of those membrane receptors and their signaling pathway have been discussed in detail in the Curcumin chapter. Because macrophage cells have surface receptors that bind to cytokines and LPS (e.g. TNFR receptor for TNF-α and TLR-4 receptor for LPS), by retaining only the cell membrane and its receptor proteins, endotoxins and cytokines can be adhered onto the membrane without additional inflammatory response, in turn, removing them from the surroundings.

According to Thamphiwatana et al., the group confirmed the preservation of various macrophage membrane proteins on the surface of the macrophage membrane coated PLGA nanoparticles, including CD14, CD284 (TLR4), CD126(IL6R), CD130, CD120a, and CD120b (TNFR1 and TNFR2), through western blotting (11). Among them, CD13 and CD284 are responsible for LPS binding; CD126 and CD130 are responsible for IL-6 binding; and CD120a and CD120b are responsible for TNF-α binding. The macrophage nanoparticles are also proven to absorb LPS, IL-6, TNF-α, and IFN-γ (11). LPS absorption is in the range of several hundred nanograms per milligram of nanoparticles, while in the cases of almost all cytokines, the absorption amount is in picograms (11).

Because their capabilities of taking cytokines and LPS away from the environment, it can have anti-inflammatory properties. The production of intracellular reactive oxygen species can be stimulated after LPS exposure. Intracellular nitric oxide (NO) production was determined for LPS stimulated J774 cells treated with PBS, PEG NP, RBC NP, and Macrophage NP (11). Among all groups, the macrophage NP group expressed the lowest amount of NO production (11). Human umbilical vein cells (HUVECs) were incubated with FITC conjugated LPS (FITC-LPS) and FITC-LPS treated with macrophage nanoparticles (11). Both fluorescent microscopy and flow cytometry results showed less fluorescent signal from the cells in FITC-LPS/macrophage NP group (11). The data implied when the surrounding LPS solution was treated with macrophage NPs, the particles absorbed majority of the LPS so that there is less FITC-LPS available for the cells to bind. Human embryonic kidney (HEK)-BLUE hTLR4 reporter cells were also used to determine the extent of TLR4 activation (11). Again, Macrophage NPs showed the lowest amount of receptor activation (11). In vivo anti-inflammatory studies also showed that Macrophage NP are able to reduce systemic inflammation in mice after tail-vein injection of LPS, with the macrophage NP reducing both TNF-α and IL-6 levels 3 hours post-injection (11). Consequently, chance of death by septic shock is also reduced compared to all other groups, shown through the survival study (11).

Membrane coating technology provides many features that can be useful for research and clinical purposes. It can become even more versatile when combining with other nanosystems, for example, the nanofibers. Cell membranes carry negative zeta-potentials, a feature that is highly exploitable for attaching cell membrane NP on to nanofibers, allow the combination of two powerful nano-systems.

Chen et al. discovered when the polycaprolactone (PCL) fibers were loaded with 1% poly-D-lysine, they were able to attract beta cell membranes and allow them to adhere onto the fiber surface (12). Fluorescent imaging, immunostaining, and bicinchoninic acid assay (BCA) have confirmed membrane loading onto the fiber surface (12). Water contact angles have also improved to show better hydrophilicity, which implies it can improve cell proliferation on the surface (12). Pancreatic beta cell lines MIN6 proliferation assay consequently showed better cell proliferation on membrane coated fibers compared to uncoated nanofibers and bare glass cover glass (12). Cell viability also improved in terms of showing higher levels of insulin secretion in the membrane coated fiber group (12). Chen et al also briefly explored the possibilities of beta cell membrane coated PLGA NPs in addition to direct membrane adhesion, and fluorescent signals confirmed similar adhering phenomenon as well (12).

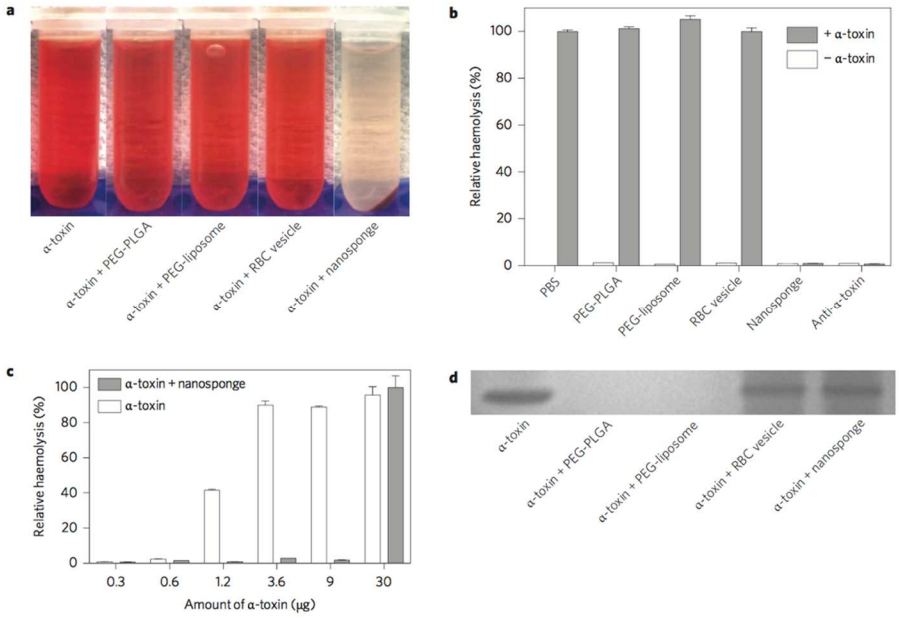

Figure 13 (7) RBC membrane coated PLGA particles are able to prevent hemolysis caused by α-toxin

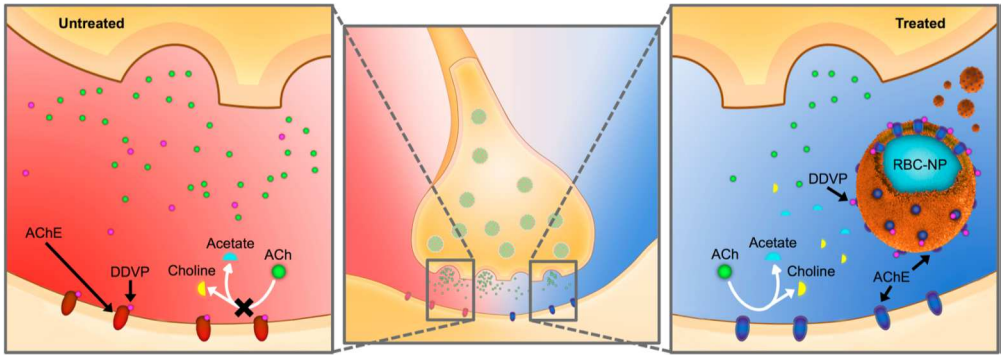

Figure 14 (11) RBC membraned coated PLGA particles can serve as a decoy binding site for DDVP, preventing the inhibition of AChE

Cell Membrane Coating and Nanofiber Attachment References

1. Abuchowski, A.; T. V. E.; Palczuk, N. C.; Davis, F. F. Journal of Biological Chemistry 1977, 252 (11), 3578–3581.

2. Zhang, F.; Liu, M.-R.; Wan, H.-T. Biological and Pharmaceutical Bulletin 2014, 37 (3), 335–339.

3. Sroda, K.; Rydlewski, J.; Langner, M.; Kozubek, A.; Grzybek, M.; Sikorski, A. F. CELLULAR & MOLECULAR BIOLOGY LETTERS 10 (2005), 37–47.

4. Tsai, R. K.; Rodriguez, P. L.; Discher, D. E. Blood Cells, Molecules, and Diseases 2010, 45 (1), 67–74.

5. Hu, C.-M. J.; Zhang, L.; Aryal, S.; Cheung, C.; Fang, R. H.; Zhang, L. Proceedings of the National Academy of Sciences 2011, 108 (27), 10980–10985.

6. Hu, C.-M. J.; Fang, R. H.; Zhang, L. Advanced Healthcare Materials 2012, 1 (5), 537–547.

7. Hu, C.-M. J.; Fang, R. H.; Copp, J.; Luk, B. T.; Zhang, L. Nature Nanotechnology 2013, 8 (5), 336–340.

8. Bhakdi, S.; Bayley, H.; Valeva, A.; Walev, I.; Walker, B.; Weller, U.; Kehoe, M.; Palmer, M. Archives of Microbiology 1996, 165 (2), 73–79.

9. Kroll, A. V.; Fang, R. H.; Zhang, L. Bioconjugate Chemistry 2017, 28 (1), 23–32.

10. Pang, Z.; Hu, C.-M. J.; Fang, R. H.; Luk, B. T.; Gao, W.; Wang, F.; Chuluun, E.; Angsantikul, P.; Thamphiwatana, S.; Lu, W.; Jiang, X.; Zhang, L. ACS Nano 2015, 9 (6), 6450–6458.

11. Macrophage Manuscript

12. Chen, Wansong, Qiangzhe Zhang, Brian T. Luk, Ronnie H. Fang, Younian Liu, Weiwei Gao, and Liangfang Zhang. "Coating nanofiber scaffolds with beta cell membrane to promote cell proliferation and function." Nanoscale 8.19 (2016): 10364-0370. Web.

Experimental Methods:

Nanofibers:

Polycaprolactone (PCL) nanofibers were prepared using the electrospinning method. The polymer crystal and ciprofloxacin were purchased from Sigma-Aldrich. Curcumin from Acros organics, and Poly-L-lysine Hydrobromide from Nordic Biolabs. PCL was dissolved in 7:3 mixture of formic acid and acetone at concentration 0.1 mg/ml. Curcumin, ciprofloxacin, and poly-L-lysine were added at concentrations 3%, 1%, and 4% to PCL weight, respectively. The content was stirred using a magnetic stir bar for 2 hours or until all solid was dissolved. Mixture was then transferred to a syringe equipped with a blunted needle (BD PrecisionGlide Needles 23G x 1 1/2). The polymer solution loaded syringe was installed on a syringe pump (New Era Pump Systems Inc). A Teflon coated Aluminum baking foil was used as the sample collector placed 12 cm away from the tip of the blunted needle. And an electric field of 20 kV was placed between the needle and the collector. Polymer solution was pumped out at a rate of 0.4 ml/hr into the electric field. After electrospinning, the sample was left to dry in the fume hood overnight. Fiber membrane sample was lifted from the collector. Fiber morphology was observed using optical microscopy (EVOS FL) and scanning electron microscopy (SEM). Fiber diameters were collected through measuring 200 randomly selected fibers samples from the SEM fiber images with ImageJ. Other polymer concentrations were also explored with their effect on fiber morphology examined using an optical microscope.

PLGA nanoparticle cores:

Poly (lactic-co-glycolic acid) (PLGA) nanoparticles were prepared using nanoprecipitation method. PLGA crystals were placed in acetone or acetonitrile solvent at concentration 20 mg/ml. DiD labeling dye was added to the mixture at ≤ 1 µg/ml concentration when DiD dye labeling was desired. The resulting content was stirred using a magnetic stir bar for 30 mins or until the content dissolves. The mixture was then pipetted rapidly to 2 ml 10mM Tris-HCl/water solution. The residual organic solvent was removed by force convection until all traces of organic solvent was evaporated. Loss volume through evaporation was re-compensated through adding additional water till a final volume of 2 ml was achieved. The final nanoparticle suspension was at 10 mg/ml and sizes are verified using dynamic light scattering (DLS).

J774 Cell Culture

A mouse macrophage cell line, J774 was purchased from Sigma-Aldrich and cultured in 10% Fetal Bovin Serum (FBS) (Hyclone) and 1% penicillin-streptomycin (Invitrogen) in Dulbecco's Modified Eagle Medium (DMEM), purchased from Invitrogen. Cells were cultured in T-175 suspension culture flasks until 90% confluency and detached by adding 2 mM EDTA/PBS solution and incubating at 37℃ for 5 mins. Harvested cells were stored at -80 ℃ in DMSO freezing medium (Sigma-Aldrich) until membrane derivation.

Cell Membrane Derivation:

Cell membrane derivation using the hypotonic lysing method. The cells were washed twice with starting buffer (20.5g sucrose, 13g sucrose, 15 ml 1M Tris-HCl, in 500 ml distilled water) and spun down at 800 rcf for 5 minutes. The pellet was washed twice

through centrifugation with isolation buffer (150 uL EGTA (ethylene glycol-bis(β-aminoethyl ether)-N,N,N',N'-tetraacetic acid) 100 mM, 100 uL protease inhibitor, and 100 uL phosphate inhibitor in 30 mL starting buffer) and homogenized using a probe homogenizer for 15 passes. The spun down pellet was re-suspended and homogenized again. All contents were centrifuged down with the ultra-centrifuge at 7,600 rpm for 25 mins (SW32Ti rotor). The supernatant was washed twice with the storage buffer (2 uM EDTA in water) using the ultra-centrifuge to spin down at 29,600 rpm for 35 mins. The membrane protein content was quantified using the bicinchoninic acid (BCA) assay.

Cell membrane coating and nanofiber attachment:

Cell membranes and PLGA nanoparticle cores were combined with the ratio of 1:1 membrane protein to polymer weight. The mixture was sonicated in a bath sonicator (Fisher Scientific) for 3 minutes or until the content was no longer opaque. Nanofiber weight was predetermined using a micro balance (####). Coated nanoparticles were then incubated with the nanofibers overnight at 37°C. The liquid was discarded and fibers washed with a sufficient amount of DI water to remove excess nanoparticles. And the NP attached nanofibers were dried in a vacuum chamber overnight.

After attachment, triplicated nanofiber samples were put in ultra-pure water and sonicated using a probe sonicator (Fisher Scientific) until the samples were broken into small pieces that disperse homogeneously in the sample solution. Then three separate liquid samples were taken out for protein content quantification using the BCA assay. The protein content was then normalized by the fiber weight.

Nanoparticle binding stability study

A triplicated set of fiber samples were placed in PBS under continuous shaking at 37°C. liquid was taken out at each time point and its protein content measured with the BCA assay. At the end of the study, each of the samples were washed using DI water and sonicated with the probe sonicator until fiber pieces are thoroughly broken down in water. Protein content was measuring with the BCA assay.

Curcumin release study

Fiber samples were put in dialysis cups (pore size: 20 kDa) and soaked in 3 L of PBS while being shielded from light and under continuous shaking. The surrounding PBS was constantly replaced with fresh PBS to minimize saturation. At predetermined time points, a set of triplicated samples was taken out and dissolved in a fixed amount of acetonitrile. A curcumin standard curve was also made using acetonitrile as a solvent. Curcumin concentration quantification was measured through determining the curcumin's fluorescent signal using a plate reader (excitation 488 nm, emission 515 nm).

Ciprofloxacin release study

A set of triplicated nanofiber samples were placed in the dialysis cups in 500 ml PBS at 37°C while being shielded from light and under continuous shaking. At predetermined time points, 100 uL of PBS was taken out of the container, and the same volume was replenished with fresh PBS. The ciprofloxacin content in each PBS sample was measured using a plate reader (excitation 272 nm, emission 448 nm). At the end of the release trial, the three fiber samples were dissolved in acetonitrile and the remaining ciprofloxacin content was also determined by reading ciprofloxacin fluorescence.

Ciprofloxacin anti-bacterial study:

The anti-bacterial study of the ciprofloxacin loaded nanofibers were measured through both inhibition in medium using optical opacity and biofilm colony size experiments.

For the inhibition study, Escherichia Coli (E. Coli) was grown in lysogeny broth (LB) overnight. The bacteria count was adjusted to 5×10^6 CFU (colony-forming unit) (0.08 OD), and 100 uL of solution was added to each clear cuvette. For the minimum inhibition concentration (MIC) study, serial dilutions of the ciprofloxacin in LB broth were added in the clear cuvettes at 1ml each. For nanofiber anti-bacteria study, nanofibers were incubated directly in 1 ml LB broth and 100 uL bacteria solution as described above. All mixtures were incubated at 37℃ for 24 hours under continuous shaking. At the end of the incubation period, fibers were removed from the medium and bacteria content in terms of optical density (OD) was measured with a biophotometer (Eppendorf D30).

For the biofilm study, E.Coli was grown overnight in LB broth then diluted to desired concentration (1.6×10^8 CFU/ml). Fiber samples were sanitized under UV light for 30 mins then placed on an agar medium plate. 5 uL of diluted culture was placed on each of the samples. Plates were incubated for 24 hours at 37℃. Samples were then transferred to a fresh agar plate and incubated again for 24 hours. The samples were vortexed to detach all bacteria and diluted culture re-seeded onto an agar plate from which the colony forming units per fiber sample were determined.

In vitro cell proliferation on nanofibers

Fiber samples were electrospun onto circular cover glass to ensure identical surface area. Human Foreskin Fibroblast (HFF) cells were seeded onto the fiber in a 12-well plate at 5×10^5 cells/well. At each predetermined time point, a triplicated sample set was trypsinized and cells removed from the fibers. The resulting cell suspension was analyzed using a hemacytometer (Fisher Scientific) for cell count. For fluorescent imaging, the cell cytoplasm was stained with Carboxyfluorescein succinimidyl ester (CFSE) before seeded into the well plate. After proliferation, cells were fixed using 10% formalin. The nucleus was stained with Hoechst fluorescent stain (Thermo Fisher). The cover slips were observed under confocal microscopy.

ROS detection using DCF-DA Assay:

Intracellular Reactive Oxygen Species (ROS) production is measured using the 2',7' –dichlorofluorescin diacetate (DCFDA) assay kit manufactured by Sigma-Aldrich. J774 macrophage cell line was used in this experiment. 2500 cells were seeded into a 96-well plate and cultured overnight. At the same time, samples were incubated with 50 ng/ml of LPS (in DMEM medium) to allow endotoxin removal by the formulation. LPS was spun down and supernatants collected. Cells were then exposed to the supernatants and incubated for 24 hours to allow sufficient ROS production. A10 mM hydrogen peroxide solution was used as the positive control. The cells were gently washed with phenol red and serum free DMEM three times and soaked in the medium for 6 hours to remove excess phenol red. After the medium was removed, DMEM containing 10 mM HEPES and 5 uM DCFDA was added to the cells and incubated for half an hour. The cells were washed for another two more times with phenol free medium. Lastly, fresh medium was placed in the

well-plate and incubated with the cells at 37°C. Fluorescence from DCF was detected using a plate reader (BioTek) (excitation: 488nm, emission: 515 nm)

Cytokine absorption:

IL-6 and TNF-α absorptions by attached macrophage nanoparticles were measured in this project. Specifically, 500 ng of IL-6 or TNF-α in 10% FBS/PBS was exposed to the formulation for 30 mins at 37 °C. The control group contained only the cytokine solution. Supernatant was taken out and spun down at 16,100 rcf for 10 mins to remove possible fiber debris and loosely attached nanoparticles. The cytokine levels in these clear supernatants were quantified using the Enzyme-linked immunosorbent assay (ELISA).

Cytokine expression using ELISA (in vitro anti-inflammatory effect)

J774 cells were seeded at 1×10^4 cells/matrix in a 96 well plate and incubated overnight to allow attaching. Formulations were also incubated with 50 ng/ml LPS in DMEM for 30 mins to allow LPS absorption. Afterwards, the fibers in each sample were collected and the liquid mixture spun down at 16,100 rcf for 10 mins. The fibers and supernatant were transferred to their corresponding wells and incubated with the cells for 8 hours. Afterwards, the medium was collected and spun down to remove any fiber and particle debris. The cytokine concentration in each medium sample was quantified using ELISA.

Results and Discussion

Characterization and formulation:

The preparation of the macrophage nanoparticle attached nanofibers (MϕNPNF) is based on well-established nanofabrication methods and involves several important steps. The mouse J774 cell line was used as a source for cell membranes. Cells were cultured and lysed for cell membranes through processes involving hypotonic lysing and ultracentrifugation. The high quality and preservation of surface receptor proteins of the membranes yielded from those processes have been confirmed by multiple sources (1), (2). PLGA polymeric nanoparticle cores, prepared using nanoprecipitation, was used as membrane structural support to keep the membranes from collapsing onto the nanofibers. Sizes of the PLGA cores were analyzed under DLS and have an average size of 80 nm. Membranes were coated onto nanofibers through sonication as previously described. The correct receptor protein orientation was also confirmed with the group's previous work (2), (3). Coated PLGA cores were again measured by DLS for diameters. An average diameter of 110 nm was obtained. Thamphiwatana et al. showed that the macrophage membrane coated cores were stable in PBS for more than two weeks (3). PCL Nanofibers were prepared from the electrospinning method with 10% polymer in solvent and yielded nanofibers containing 3% (w/w) curcumin and 1% (w/w) ciprofloxacin. Macrophage membranes coated nanoparticles (MϕNP) were incubated with nanofibers for 1 hour, after which excess and loosely attached nanoparticles were washed away using deionized water. Attachment is confirmed using fluorescent microscopy while MϕNPs are labeled with dye DiD and nanofiber are detected using curcumin's fluorescence (Figure 15). After

incubation and washing, fluorescent images with curcumin fluorescence (GFP channel Figure 15 left) in nanofibers and DiD fluorescence (CY5 channel Figure 15 middle) in the nanoparticles confirmed the co-localization of the nanoparticles and nanofibers (dual channel overlay Figure 15 right), with DiD signals spreading along the nanofibers. The fluorescent results indicate nanofiber surface binding of the nanoparticles. SEM images further confirmed the attachment by visually capturing individual nanoparticles on the nanofiber surface (Figure 16). SEM images show that nanoparticle attachment preserved the fibers' smooth and fibrous morphology. Through observing the SEM microscopy images, one can conclude that the diameter distribution the fibers follows the typical Gaussian distribution with the mean at 135 nm, median 126 nm, and standard deviation 43 nm (Figure 17).

Poly-L-lysine is the main component in the fibers to attract cell membrane coated nanoparticles. All membrane proteins have negative zeta-potentials. Poly-L-lysine provides positively charged groups for the membrane proteins to interact through electro-static interaction. The same principle was also used in cell culture flasks, which are treated with Poly-lysine at the bottom to provide more available sites for cell adherence. Since the cell membrane coated nanoparticles preserve most or all surface membrane proteins, similar electrostatic interactions should be expected from the coated nanoparticles. Therefore, poly-L-lysine loaded nanofibers should have the advantage of increasing the number of binding sites to the nanoparticles, though too much poly-L-lysine loading may affect fiber morphology because electrospinning depends strongly on the solution's viscosity. PCL polymer solutions were then added increasing amount of poly-L-lysine, and

the fluorescent images in Figure 18 showed no significant morphological effect when fibers are loaded up to 4% (w/w) poly-lysine.

The loading test was done by detecting the amount of nanoparticle loading through incubating concentrated MϕNP suspension (3.33 mg/ml polymer weight) with the nanofibers. After washing with distill water to remove excess nanoparticles, the fibers were then homogenized in fresh water using a probe sonicator until the fiber pieces are small and homogenously suspending in water. Protein concentration in the homogenized samples were then quantified using the BCA assay. 0%, 1% and 4% (w/w) poly-lysine loadings were used in the test (Figure 19). 0% yielded less than 1% average nanoparticle loading. This is simply due to the lack up binding sites for charge interaction on the fibers. 1% polylysine showed a slight but insignificant increase. Lastly 4% poly-lysine was able to retain up to 10% nanoparticles. Loading test clearly showed an increasing amount of retained nanoparticles from increasing amount of particle loading.

Nanoparticle stability and drug release:

The stability of the electrostatic interactions in PBS was measured. Samples were incubated with 1x PBS at 37 C under continuous shaking for 3 days. And at predetermined time points, a triplicated set of fiber samples was taken out of the buffer solution and homogenized with a probe sonicator. The BCA assay was used to detect the protein content in the homogenized solution. The poly-L-lysine loaded fibers provide an excellent platform to retain the nanoparticles. From the results in Figure 20, the system presented negligible nanoparticle loss in the first 24 hours. Noticeable release occurred between 24 and 72 hours. After 48 hours, the system loses about half of the all attached nanoparticles. After 72 hours,

the final retained nanoparticles decreased to $2.19 \pm 1.00\%$ (w/w) of the fiber weight. Fortunately, endotoxin and cytokine bindings usually complete within 30 minutes of contact. Therefore, the particle retention provides enough time to absorb pro-inflammatory cytokines at the site of nanofiber implantation.

The antibiotic ciprofloxacin was loaded 1% (w/w) to fiber weight and its release mechanism was investigated by incubating known amount of fiber samples with 100 ml PBS under 37 C. The solution was constantly stirred. The change of ciprofloxacin fluorescent signal was observed and the absolute amount quantified with a standard curve. The amount of drugs within the fibers before and after the release trial was quantified by dissolving the fibers in acetonitrile and measuring fluorescent signal. The results are shown in Figure 22. The system releases about half of its loaded drug in merely 1 hour and up to 75% after 2 hours. Within 24 hours, the system releases up to 100% of the drug. After 36 hours, all tested samples contained barely detectable amount of ciprofloxacin in the fibers. Ciprofloxacin released quickly from the nanofiber mesh mainly due to its solubility in water and lack of retention component in the formulation.

The release of the third component in the system, curcumin, was measured by incubating the multiple samples in the dialysis cups and dialyze against large volumes of PBS. All samples were shielded completely from light. At each time point, a set of triplicated samples were taken out of the container and dissolved in acetonitrile. The fluorescent signal was observed and quantified using a free curcumin standard curve. The experiments were done in both 25 C and 37 C under continuous shaking. Results can be seen in Figure 21 Curcumin has minimal solubility in water so the release of curcumin is

mainly dominated by solid diffusion, and the mechanism can be strongly depended on temperature. At 25 C, samples showed negligible release at the end of 48 hours. The curcumin content in all tested sample showed little to no statistical difference from each other. However, when the release condition was changed to 37C, the diffusion mechanism dramatically sped up. The results showed an initial burst release of curcumin in the first 12 hours with the concentration reaching below 50% of the original value after just 9 hours. After the burst release, it leveled off and released the drug relatively more slowly. At the end of 48 hours, overall retention of the drug was about 11.8 ± 3.9 %. Overall, the release of curcumin was significantly shower than ciprofloxacin due to its lower water solubility.

Anti-bacterial efficacy of ciprofloxacin (Figures 24 and 25):

Ciprofloxacin is a powerful antibiotic with significantly more efficacy and wider spectrum of activity than other common antibiotics such as norfloxacin and nalidixic acid (4). In fact, three major components in the nanofibers formulation are reported to have anti-microbial efficacy. According to Y. Wang et al., curcumin is effective against various kinds of bacteria and has even more efficacy against fungi than bacteria (5). However, it has a very high mean inhibition concentration (MIC) of 250 μg/ml against E. Coli, a common gram-negative bacterium (5).

Poly-L-lysine was also found to be anti-bacterial. The chemical is effective against many strains of gram-negative and gram-positive bacteria, including E. coli and S. aureus (6). Moreover, the conformation of the molecular structure can impact its efficacy significantly. Shima et al. discovered that ϵ-poly-L-lysine ϵ-PL is a lot more effective against all bacteria than α-poly-L-lysine (6). The MIC of ϵ-PL was checked by adding

serial diluted poly-lysine formulation into 5×10^5 CFU/ml E. coli in LB broth, and shaken overnight. Bacteria growth is quantified through observing optical density (O.D.). Unfortunately, ϵ-PL yielded relatively high MIC against E. Coli, with the estimated MIC at over 50 μg/ml. At 4% (w/w) poly-L-lysine loading, it is unlikely to show significant anti-bacterial efficacy from the fibers with the component alone.

The same inhibition study was done with Ciprofloxacin as well. Being a highly effective anti-biotic, ciprofloxacin showed dramatically lower MIC to E. coli than either of the other components in the system at < 0.1 μg/ml. Given the nature of the drug's release property as mentioned above, a minuscule amount of loading would be sufficient to inhibit the growth of E. Coli. After the formulation titration, the MIC of ciprofloxacin is found to be < 0.1μg/ml, which is 10 times lower than ϵ-poly-L-lysine and 2500 times lower than curcumin.

To observe the anti-bacterial effect of the loaded ciprofloxacin, three groups of triplicated nanofiber samples, poly-lysine only, poly-lysine with curcumin, and poly-lysine with curcumin and ciprofloxacin, were incubated with 5×10^5 CFU/ml E. coli at 37C under continuous shaking. The O.D. was observed after 24 hours. Even though poly-L-lysine's anti-microbial effect is well-documented, 50 μg/ml is well beyond the loading amount a 1 mg fiber sample could provide. Also, as expected, due to the high MIC of Curcumin to E. coli and its poor solubility in water, the formulation does not provide enough of the drug to inhibit bacteria growth. The antibiotic loaded sample could fully inhibit E. coli in LB broth, thanks to fibers' fast release mechanism of ciprofloxacin and the drugs low MIC value to E Coli.

The surface anti-microbial effect of the nanofibers was tested using E. coli biofilm. 1×10^5 CFU E. coli was seeded on each of the fiber samples. The bacteria were grown on the sample surface overnight. At the end of the trial period, all samples were sonicated in LB broth to detach the bacteria and transferred to another agar plate to quantify colony counts. Poly-L-lysine only, and curcumin loaded fibers are not able to reduce bacteria growth in dry conditions either, despite of the lower liquid volume and higher local concentration compared to the previous study. Meanwhile, similar to the previous experiment, ciprofloxacin again provided the benefit of completely inhibiting and killing E. coli on the fiber surface, which almost no bacteria colony observed. Such property is especially useful when the system is used as a topical wound dressing. The added antibiotic is able to reduce or prevent bacteria growth at the wound site and hence reduce chances of infection.

In vitro cell proliferation study (Figure 23):

Nanofibers are known to promote cell proliferation. As discussed in the previous sections, nanofibers provide a scaffold that mimics the extracellular matrix during wound healing process. As a result, cells are able to adhere and migrate more efficiently on the matrix. The poly-L-lysine component in the fibers is also able to enhance cell recruitment and attachment, similar to a tissue culture treated polystyrene flask.

In order to further verify the system's capability to promote cell growth, human foreskin fibroblasts (HFF) were grown on the fiber surface. Surface area was controlled by electrospinning fiber sample directly onto a confocal cover slip (2 cm diameter) and using a bare cover glass slip as control. HFF cells were seeded onto the cover slips at 5×10^4

cells/matrix into a 12-well plate. Samples were taken every 24 hours by detaching cells using trypsin and counting with a hemacytometer.

Due to the excellent biocompatibility and fibrous structure of the nanofibers, HFF cells are able to proliferate well onto the sample surface. The cell count showed a significant boost of attached cells onto the nanofiber than bare cover slip (control group) alone. The difference in cell numbers became apparent after 24 hours of culture. After 72 hours, the cells from the nanofiber group had almost 50% more cells than the control group, with more than 1.6×10^5 cells compared a mere 1.1×10^5 cells in the control group. Moreover, though the nanoparticles should not benefit cell proliferation, they have no negative impact on cell proliferation when integrated onto the fibers. The MϕNP attached nanofiber group showed no statistical difference in cell count with the nanofiber only group.

To visually observe the attached cells, HFF cells are stained with CFSE and Hoechst stain and imaged under confocal microscopy and imaged after 24 and 48 hours. Same trend can also be observed in the confocal images.

In Vitro Cytokines and Endotoxin Neutralization (Figures 26 and 27)

Macrophage cells have surface protein receptors that signal complicated pathways to enable the transcription of pro-inflammatory cytokines. As mentioned previously, cell membranes derived from hypotonic lysing can preserve those membrane receptors and therefore allow us to coat those receptors onto nanoparticles. Macrophage membranes coated nanoparticles have already been reported to neutralize endotoxin and cytokines both in vitro and in vivo.

Additionally, the system's principle to retain nanoparticles is through interacting the positively charged poly-L-lysine in fibers with negatively charged cell membrane proteins on the coated nanoparticles. Meanwhile, most cytokines are also negatively charged, just as the membrane receptors. It is reasonable to predict that similar interactions can exist between poly-L-lysine and cytokines. Fibers should also be able to neutralize the cytokines as well.

To verify the hypothesis, two types of cytokines, TNF-α and IL-6, were incubated with triplicated samples of 1 mg particle attached nanofibers and results were compared with incubation with blank control (no treatment) and 1 mg bare nanofibers. Samples were tested for cytokine concentration before incubation with ELISA. The rest of cytokine was incubated with the three groups at 37C for 30 mins. Afterwards, the solution was collected and spun down for excess nanoparticles. Concentrations of cytokines in the supernatant was quantified again using ELISA. The results were compared to the values before treatment.

As expected, poly-L-lysine fibers are able to reduce cytokine levels in both cases. In the case of TNF-α, there was a slight reduction of TNF-α after incubating with bare-fibers without nanoparticles. The surface charge of poly-lysine attracted about 20% of the 600 pg/ml TNF-α input. When the system is attached with macrophage nanoparticles, the level further reduced to below 200 pg/ml. Clearly, the addition of nanoparticles in the sample provided an additional boost of neutralizing cytokines, thanks to the TNFR receptors on the nanoparticle surface. Meanwhile, using nanoparticles alone was also able

to neutralize similar amount of TNF-α, showing that the effect of poly-L-lysine is dominated by the efficacy of the nanoparticles.

However, when the system was in contact with IL-6, the results showed that the polylysine is able to neutralize the majority of the cytokines and that attaching the nanoparticles offered no statistical difference compared to the fiber alone. This means IL-6 has greater affinity to the positive charge sites than TNF-α possibly due to carrying different zeta-potential.

The cytokine neutralization experiments showed that the system was able to effectively reduce the levels of the cytokines in vitro through both specific receptor binding and non-specific electrostatic interactions.

In vitro anti-inflammatory efficacy of curcumin (Figure 28)

The in vitro anti-inflammatory efficacy of curcumin was investigated using J774 macrophage cells. 1×10^4 cells/well were seeded into a 96-well tissue culture plate and cultured overnight. 50 ng/ml of LPS was introduced into each well followed by adding the treatment groups: no treatment, free curcumin, curcumin loaded nanofibers, and curcumin loaded nanofibers with nanoparticles. The mixtures were incubated for 12 hours. At the end of the incubation, the supernatant from each well was taken out and centrifuged to remove loose nanoparticles and fiber debris. The inflammatory cytokine IL-6 was quantified using ELISA.

According to the results, 50 ng/ml of LPS successfully induced inflammatory response of the J774 cells, with the cells in LPS group expressing three times as much IL-

6 levels than the blank control. Free curcumin is known to interfere with the NF-κB activation process and inhibit cytokine transcription. Therefore, the cellular inflammation was almost completely avoided by free curcumin. The twelve-hour incubation period allows the majority of curcumin to be released (see curcumin release profile), hence the released curcumin was also able to modulate inflammation through similar process of signaling pathway mediation as the free curcumin group. Lastly, due to the effective potency of curcumin, the nanoparticles fell short in terms of the efficacy. The hybrid group showed no added effect from curcumin nanofiber only group.

In vivo macrophage recruitment study (Figure 29)

The macrophages ability to absorb pro-inflammatory cytokines can reduce the inflammation phase of wound healing by reducing local cytokine levels and immune cell recruitment.

To investigate the reduction of macrophage recruitment efficacy of our system, two non-adjacent 6-mm-diameter skin wounds were created on the lower back of each C57 BL mouse. Formulations were applied directly onto the wounds. After 5 days, the wound and surrounding tissue were collected and stained with anti-mouse CD68 then with Dylight 649 anti-mouse IgG secondary antibody then mounted with DAPI.

According to our results, the retained NPs in the NFs were able to reduce macrophage recruitment by almost half due to their cytokine neutralization properties. Drug loaded nanofibers provided an even greater amount of macrophage recruitment reduction by directly interacting with the NF-κB activation process and many other wound healing related processes discussed in the previous sections.

Results and Discussion References

1. Chen, Wansong, Qiangzhe Zhang, Brian T. Luk, Ronnie H. Fang, Younian Liu, Weiwei Gao, and Liangfang Zhang. "Coating nanofiber scaffolds with beta cell membrane to promote cell proliferation and function." Nanoscale 8.19 (2016): 10364-0370. Web.
2. S. Thamphiwatana manuscript: Biomimetic macrophage-like nanoparticles for sepsis management
3. Hu, Che-Ming J., Ronnie H. Fang, Brian T. Luk, Kevin N. H. Chen, Cody Carpenter, Weiwei Gao, Kang Zhang, and Liangfang Zhang. "'Marker-of-self' functionalization of nanoscale particles through a top-down cellular membrane coating approach." Nanoscale 5.7 (2013): 2664. Web.
4. Zeiler, H.-J.; Grohe, K. Ciprofloxacin 1986, 14–18.
5. Wang, Y.; Lu, Z.; Wu, H.; Lv, F. International Journal of Food Microbiology 2009, 136 (1), 71–74.
6. Shima, S.; Matsuoka, H.; Iwamoto, T.; Sakai, H. The Journal of Antibiotics 1984, 37 (11), 1449–1455.

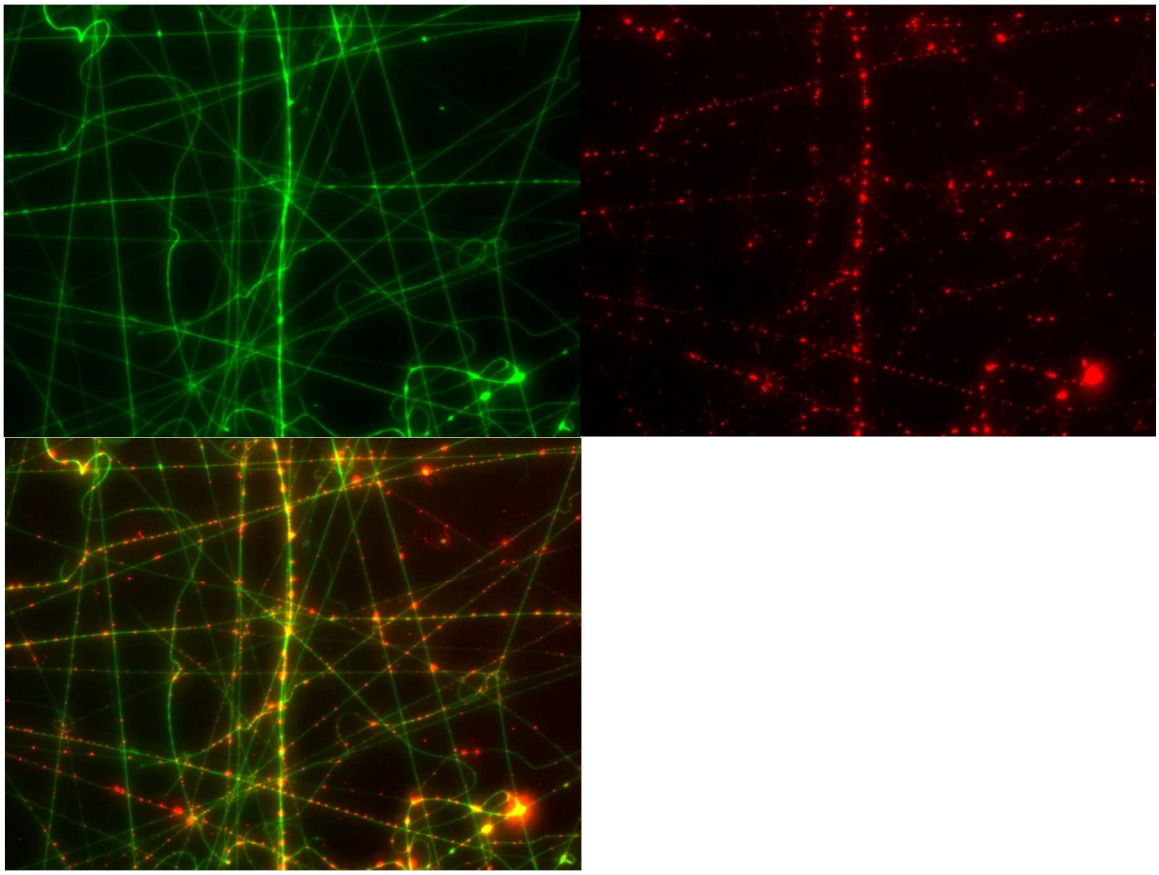

Figure 15 fluorescent images of the hybrid system. Top left: curcumin in fiber (GFP). Top right: Attached nanofibers (DiD, CY5). Bottom: merged.

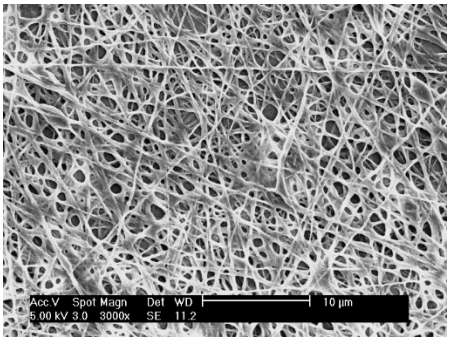

Figure 16 SEM image of the electrospun PCL nanofibers

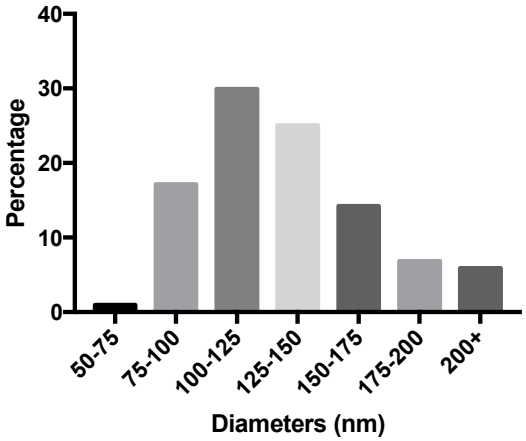

Figure 17 nanofiber diameter distribution

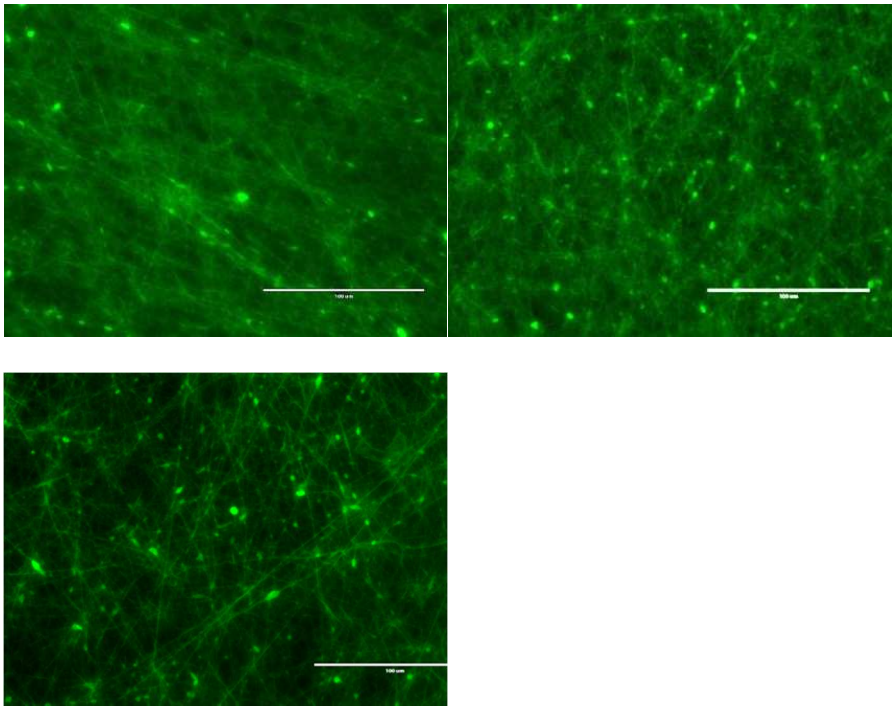

Figure 18 polylysine loading on fiber morphology

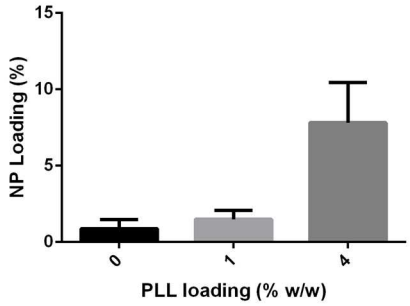

Figure 19 polylysine (PLL) loading on nanoparticle loading

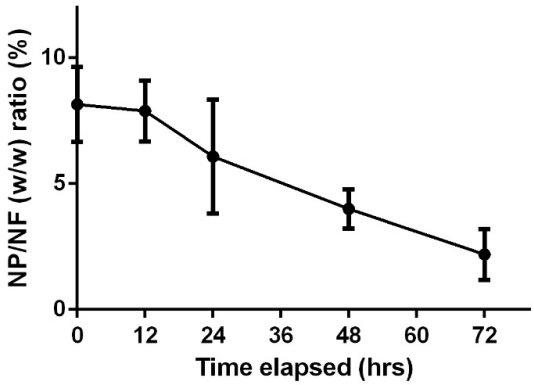

Figure 20 nanoparticle retention in 72 hours.

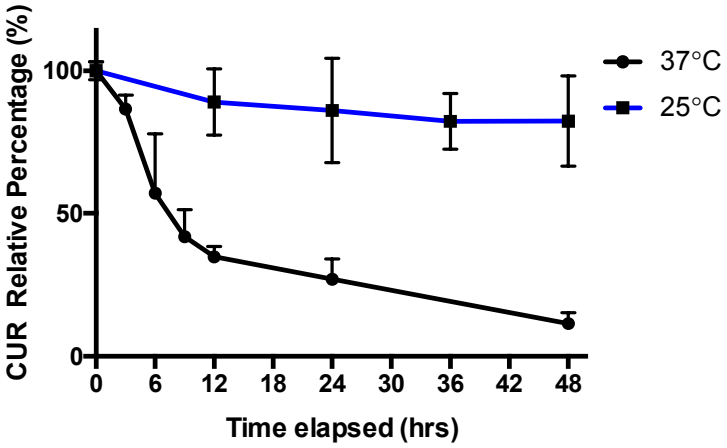

Figure 21 curcumin release at 25 C and 37 C in 48 hours

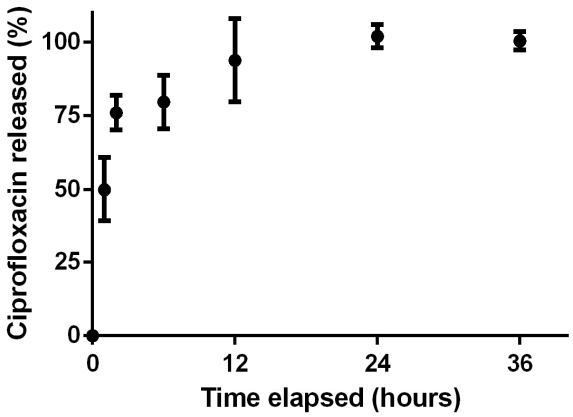

Figure 22 ciprofloxacin release in 36 hours

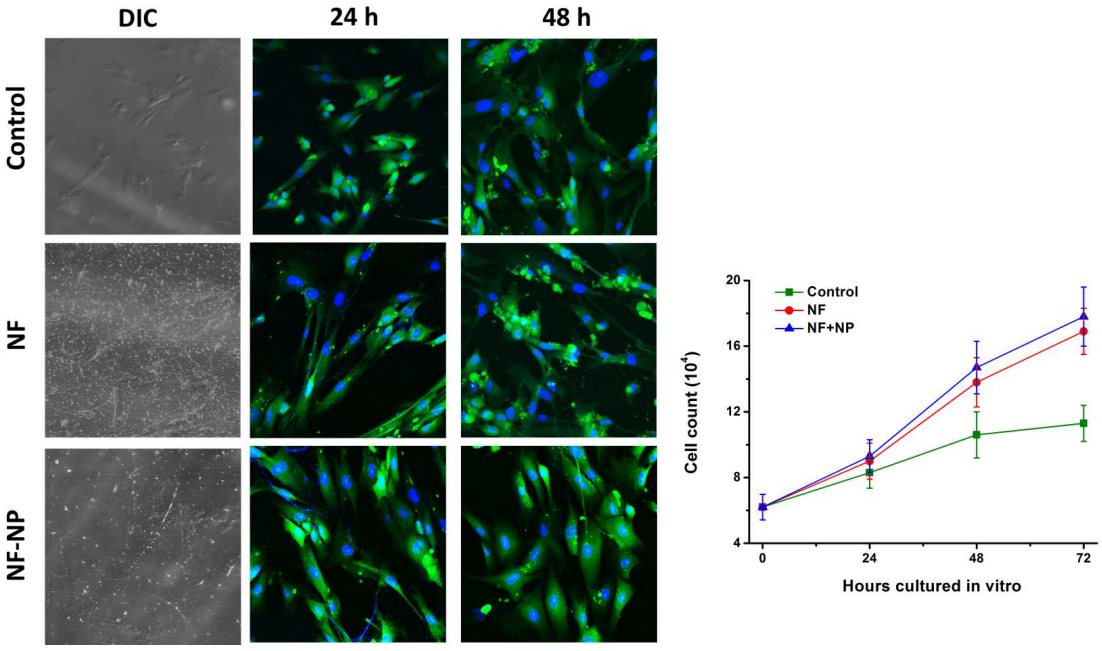

Figure 23 Human foreskin fibroblast (HFF) cell proliferation of nanofibers. Left: confocal images of proliferated cells. Right: cell count during 72 hours.

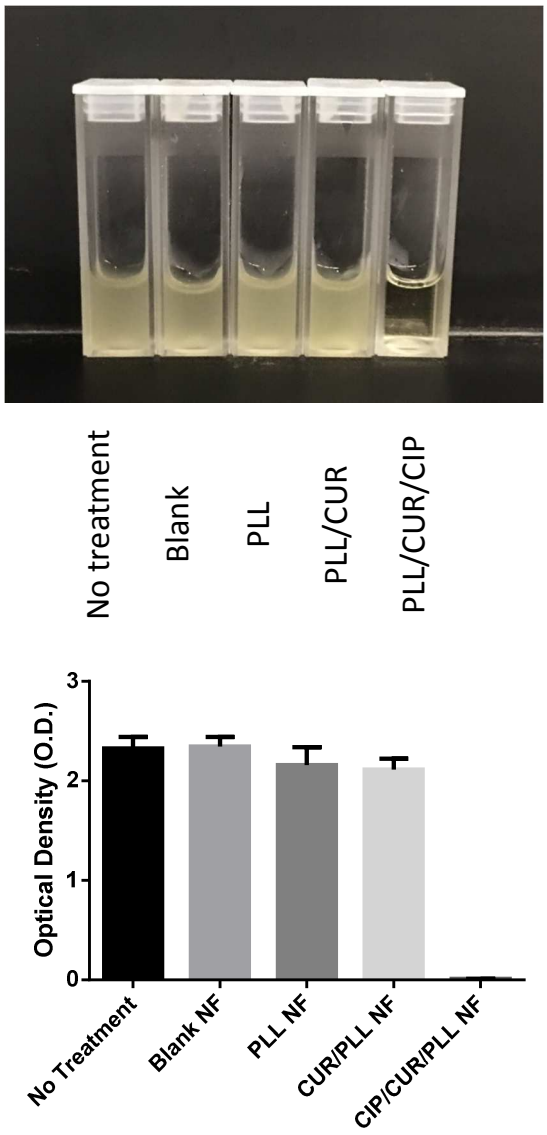

Figure 24 In vitro bacteria inhibition efficacy of ciprofloxacin loaded nanofibers against E. Coli.

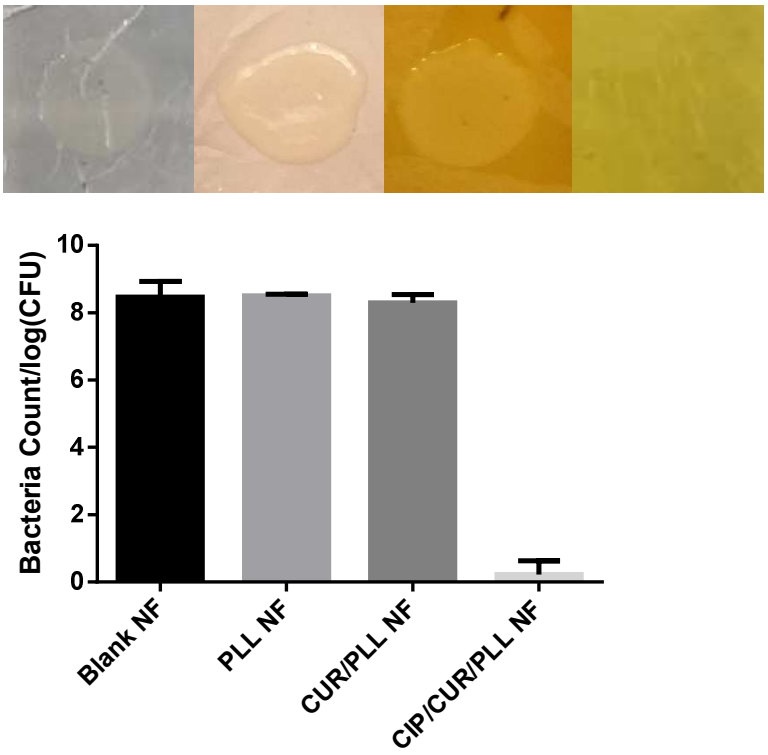

Figure 25 In vitro biofilm inhibition efficacy of ciprofloxacin loaded nanofibers against E. Coli

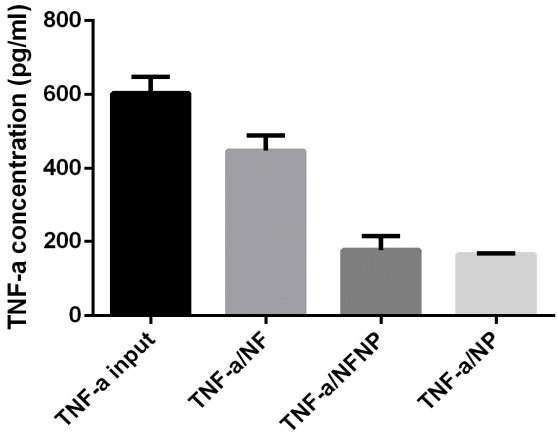

Figure 26 In vitro TNF-α neutralization with MϕNP loaded Nanofibers

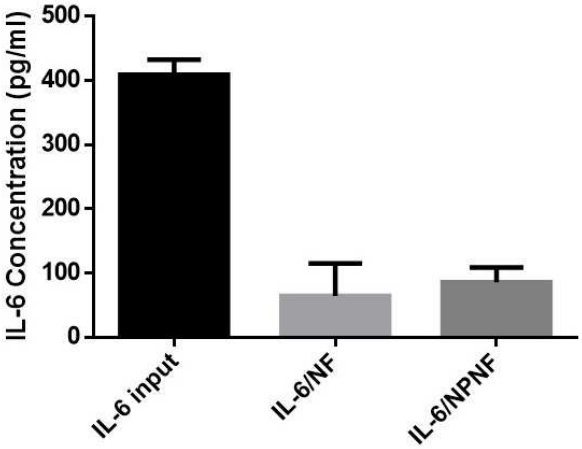

Figure 27 In vitro IL-6 neutralization with MϕNP loaded Nanofibers

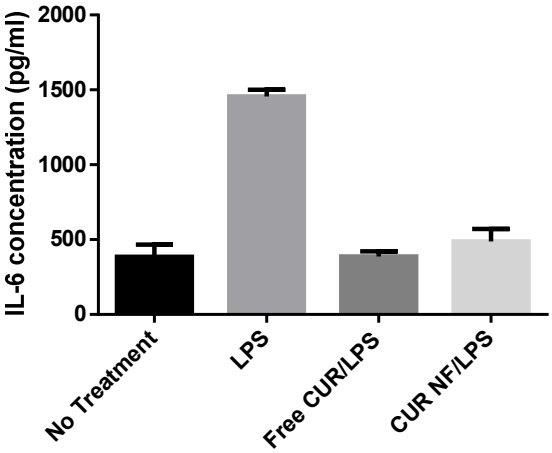

Figure 28 In vitro anti-inflammatory efficacies of Curcumin on J774 macrophage cells

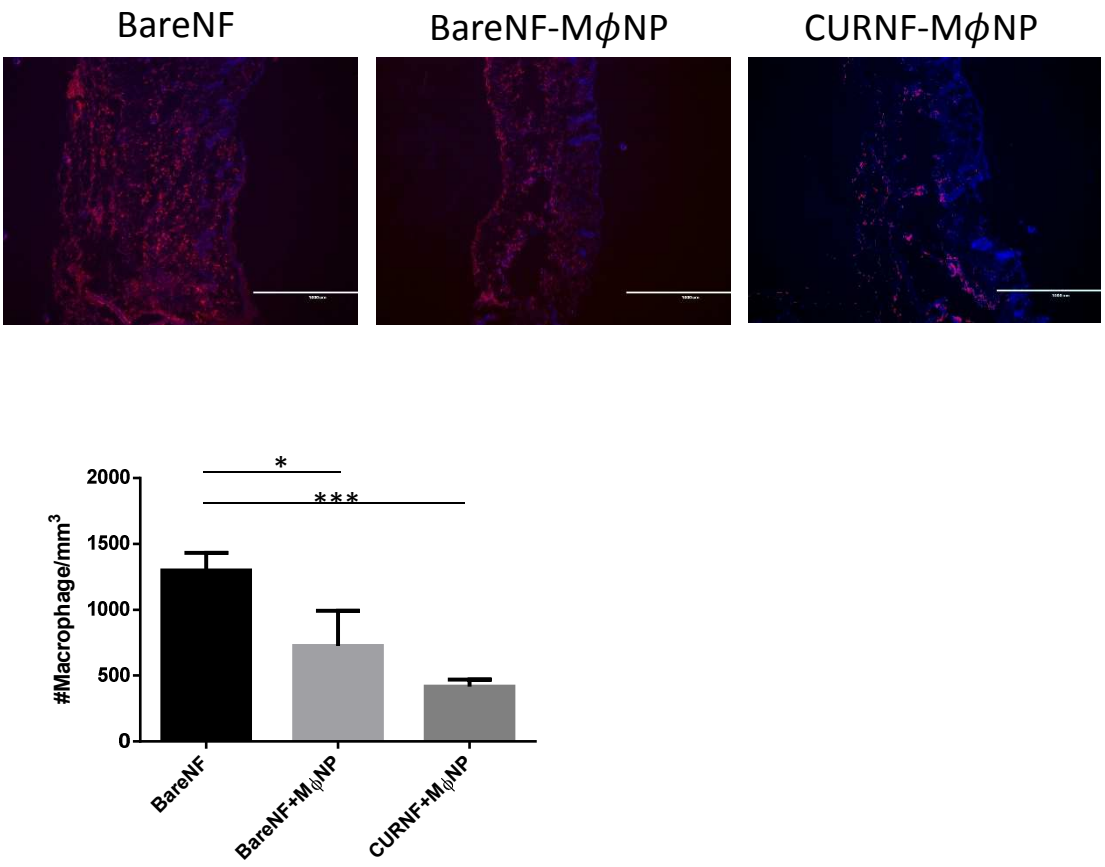

Figure 29 In vivo macrophage recruitment reduction of fiber retained MϕNP and curcumin loaded nanofibers.

Conclusion:

Nanofibers became the area of intense research after their appealing properties were discovered. High surface area and porosity allows biocompatibility and make them an excellent platform for drug delivery. Its structure mimics the natural extracellular matrix during wound closure. Their highly customizable surface can be tailored to fit various needs. Because of their unique physical properties, their drug delivery applications and wound healing efficacies have been well-documented in literature. The project was designed to take advantage of those fascinating properties of the nanofibers and explore the possibility of combining the polymeric fibers with the newly arose cell membrane coating technology, while at the same time, use them as a traditional drug delivery medium. By incorporating three different components into the polymeric fiber matrix, we built a biomimetic hybrid system that modulates inflammation in three major aspects: using macrophage membrane coated nanoparticles to neutralize pro-inflammatory cytokine secretion to reduce unwanted immune cell recruitment; releasing anti-inflammatory drug, curcumin, to reduce the production of cytokines through interfering with the activation of NF-κB; and inhibiting the growth of gram-negative bacteria to further reduce the production of endotoxin, which is responsible for inducing chronic inflammation in vivo. The three features of the hybrid system were successfully demonstrated in the project. Since the system is designed to reduce inflammation and promote surface cell proliferation, it can be used as a powerful treatment for wound healing. However, due to the complex nature of in vivo cutaneous wound healing, such in vivo experiment was not pursued. Further investigation will be conducted to observe the wound healing in mouse model.